Tectonophysics 692 (2016) 164–180

Contents lists available at ScienceDirect

Tectonophysics

journal homepage: www.elsevier.com/locate/tecto

Crustal structures from the Wuyi-Yunkai orogen to the Taiwan orogen: The onshore-offshore wide-angle seismic experiments of the TAIGER and ATSEE projects

Yao-Wen Kuo [a], Chien-Ying Wang [a], Hao Kuo-Chen [a,*], Xin Jin [b,c], Hui-Teng Cai [b,c], Jing-Yi Lin [a], Francis T. Wu [d], Horng-Yuan Yen [a], Bor-Shouh Huang [e], Wen-Tzong Liang [e], David Okaya [f], Larry Brown [g]

[a] Dept. of Earth Sciences, National Central University, Zhongli, Taiwan
[b] College of Civil Engineering, Fuzhou University, Fuzhou, China
[c] Earthquake Administration of Fujian Province, Fuzhou, China
[d] Dept. of Geological and Environmental Science, State University of New York at Binghamton, Binghamton, USA
[e] Institute of Earth Sciences, Academia Sinica, Taipei, Taiwan
[f] Dept. of Earth Science, University of Southern California, Los Angeles, CA, USA
[g] Dept. of Earth and Atmosphere Science, Cornell University, Ithaca, NY, USA

ARTICLE INFO

Article history:
Received 8 March 2015
Received in revised form 9 August 2015
Accepted 20 September 2015
Available online 30 September 2015

Keywords:
Wuyi-Yunkai orogen
Taiwan orogen
Taiwan Strait
Onshore-offshore wide-angle seismic profile
Ray tracing

ABSTRACT

Knowledge of the crustal structure is important for understanding the tectonic framework and geological evolution of southeastern China and adjacent areas. In this study, we integrated the datasets from the TAIGER (TAiwan Integrated GEodynamic Research) and ATSEE (Across Taiwan Strait Explosion Experiment) projects to resolve onshore-offshore deep crustal seismic profiles from the Wuyi-Yunkai orogen to the Taiwan orogen in southeastern China. Three seismic profiles were resolved, and the longest profile was 850 km. Unlike 2D and 3D first arrival travel-time tomography from previous studies, we used both refracted and reflected phases (Pg, Pn, PcP, and PmP) to model the crustal structures and the crustal reflectors. In total, data from 40 shots, 2 earthquakes, and approximately 1,950 stations were used; 15,612 arrivals were selected among three transects. Using these data, we determined the complex crustal evolution since the Paleozoic era , involving the closed Paleozoic rift basin in central Fujian, the Cenozoic extension due to the South China Sea opening beneath the coastline of southern Fujian, and the on-going collision of the Taiwan orogen. The shape of the Moho, which also reflects the crustal evolution, can be summarized as follows: ~30 km deep to the west of Fujian, deepening toward central Fujian (~35 km), becoming shallower toward the Taiwan Strait (~28 km), deepening again toward the mountain belt of Taiwan (~42 km), and becoming shallower toward the Pacific Ocean (~10 km).

1. Introduction

Knowing the crustal structure is important for understanding tectonic frameworks and geological evolution, especially for the complicated tectonic history of southeastern China and its adjacent areas (Fig. 1). The crustal evolution in southeastern China began in the Neoproterozoic when the paleo-South China ocean plate subducted under the Yangtz block, which subsequently caused a collision between the surrounding continents to form the South China continent. Then, the South China continent was separated again by the worldwide breakup of the Rodinia Supercontinent (Shu, 2012). After the breakup, the 2 microcontinents within the Cathaysia block collided with each other in the Cenozoic (Xu et al., 2007). Overall, it is generally believed that the current tectonics in the Fujian area were created by the westward underplating of the paleo-Pacific plate into the Eurasian plate (Mao et al., 2014). In Taiwan, the orogeny was created by the oblique collision between the Eurasian and Philippine Sea plates in the Neogene (Suppe, 1984). The Philippine Sea plate is moving northwest with a velocity of 8.2 mm/yr based on the GPS data (Yu et al., 1997).

In the past few decades, many geophysical studies have investigated this region to understand the mechanism of crustal evolution using 3D seismic travel-time tomography (e.g., Roecker et al., 1987; Rau and Wu, 1995; Ma et al., 1996; Kim et al., 2005; Wu et al., 2007; Kuo-Chen et al., 2012a,2012b; Zheng et al, 2013; Huang et al., 2014; and Cai et al., 2015). First, Roecker et al. (1987) showed the structure of the subduction zones of the Eurasian and Philippine Sea Plates based on the results from both tomography and seismicity. Rau and Wu (1995) noted that the crust in Taiwan is thickened to form a root, probably as a result of deformation in the lithospheric scale, based on the tomographic results from earthquake data. Then, via the use of denser seismometer

* Corresponding author at: Dept. of Earth Sciences, National Central University, No. 300, Zhongda Rd. Zhongli District, Taoyuan City, 32001, Taiwan.
E-mail address: kuochen@ncu.edu.tw (H. Kuo-Chen).

http://dx.doi.org/10.1016/j.tecto.2015.09.014
0040-1951/

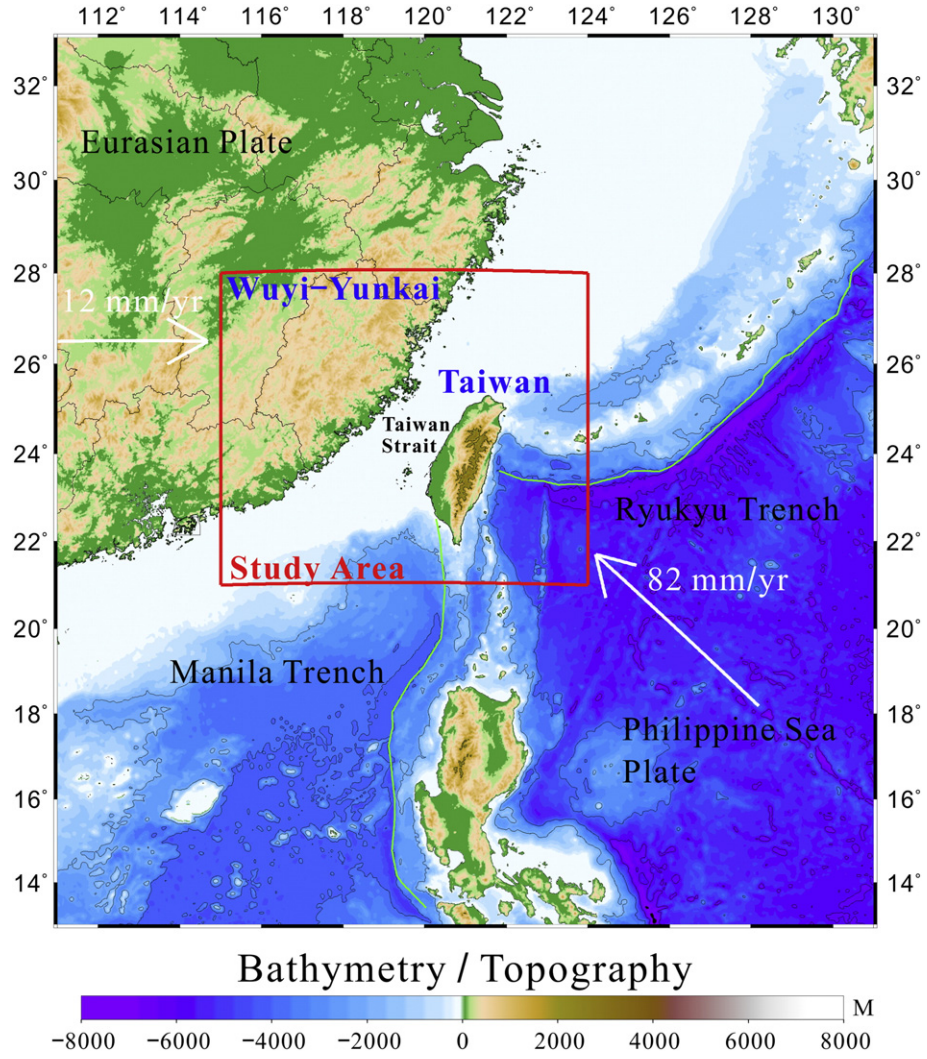

Fig. 1. The tectonic settings in the vicinity of Taiwan. Taiwan is at the convergent boundary of the Eurasian Plate and the Philippine Sea Plate (white arrow in the NW direction). In addition, the Fujian area of the Eurasian Plate is also under the push force from the Indian Plate (direction of the white arrow). The green lines mark the locations of the Ryukyu Trench and the Manila Trench. The red rectangle marks the study area. The blue characters represents 2 major mountain belts in this area.

arrays for capturing P- and S-wave data, Kim et al. (2005) constructed a better crustal velocity structure. To better constrain the velocity model at shallow depths, Wu et al. (2007) proposed a model using the data from CWBSN with TSMIP to construct the 3D Vp and Vp/Vs velocity model. Using data from both passive and active sources, including teleseismic data, Kuo-Chen et al. (2012a) resolved 3D Vp and Vp/Vs models down to 200 km in depth beneath Taiwan and found 2 crustal roots beneath the mountain ranges (the Central and Coastal Ranges) in their models. Kuo-Chen et al. (2012b) further explained that the low-velocity area with the lack of seismicity is caused by an α-β quartz transition instead of high fluid pressure or partial melting in the mid-crust in the Central Range. Zheng et al. (2013) used teleseismic data to construct a Vp model down to a depth of 400 km in southeastern China, covering the Fujian range, Taiwan Strait, and Taiwan. Huang et al. (2014) used unprecedented S-wave data with P-wave and S-P time data in a joint-inversion scheme to better constrain the westernmost Philippine Sea Plate edge. Cai et al. (2015) used data from active sources and earthquakes to resolve the velocity structure of the Zhenghe-Dapu fault zone in the middle of Fujian. However, in the studies in this region, most seismic travel-time data from earthquakes for seismic tomography were from the Central Weather Bureau (CWB), which only resolved the seismic imaging in Taiwan (e.g., Roecker et al., 1987; Rau and Wu, 1995; Ma et al., 1996; Kim et al., 2005; and Wu et al., 2007). In contrast, Cai et al. (2015) used active and passive sources to image the crustal structure only in Fujian from the data set of the Earthquake Administration of Fujian Province (EAFP). In addition, Zheng et al. (2013) only used teleseismic events from the data sets of CWB and EAFP to resolve the upper mantle structure from the Fujian province to Taiwan. Overall, most studies resolved the subsurface only for the Taiwan region and its offshore areas or only for southeastern China. They did not discuss the tectonic relationship between southeastern China (Fujian province) and Taiwan because of the limited data sets. The crustal evolution from southeastern China to Taiwan is still poorly understood.

To obtain 2D high-resolution seismic imaging of the crustal structure in Taiwan and its offshore areas, the Taiwan-USA collaborative onshore-offshore seismic research project, TAICRUST, was carried out in 1995 (e.g., Shih et al., 1998; Yeh et al., 1998; and McIntosh et al., 2005). Although it was a fruitful experiment, owing to the active sources (air guns) mainly from the eastern areas offshore of Taiwan, the depth resolution was limited to above 20-30 km (McIntosh et al., 2005). After TAICRUST, in 2004, a more comprehensive Taiwan-USA collaborative research project, Taiwan Integrated Geodynamic Research (TAIGER), was conducted to improve the resolution of the crustal and upper mantle structure using improved instrumentation and analysis techniques, which involved both active and passive seismic experiments (e.g., Kuo-Chen et al., 2009, 2012a,2012b, 2013; Lester and McIntosh, 2012b; McIntosh et al., 2012, 2013, 2014; Lester et al., 2013; Eakin et al, 2014; and Van Avendonk et al., 2014). The detailed experimental

design and geophysical results from this project were reviewed by Wu et al. (2014).

In recent decades, researchers have studied subsurface structures from 2D onshore-offshore wide-angle seismic deep profiles using the data from the TAICRUST project and found some important results, such as those from Shih et al. (1998), Yeh et al. (1998), and McIntosh et al. (2005). The Pg, Pn, PcP, and PmP phases can be obtained from these data (Yeh et al., 1998). The variation in the crustal thickness shows a specific pattern from Taiwan, the Hsincheng Ridge (~45 km east to Taiwan), to the Hoping and Nanao Basins (Shih et al., 1998). In addition to land explosions, marine airguns are important sources for the datasets in this experiment. McIntosh et al. (2005) integrated the onshore and offshore datasets and proposed an evolution model involving a thinned-skin process from the south to lithospheric-scale collisions in the north, with the Hengchun Peninsula being at the stage of incipient subduction.

Recent studies of the 2D wide-angle data in this area are based on the results from the TAIGER project (e.g., Lester et al., 2012a, 2013; McIntosh et al., 2012, 2013, 2014; Eakin et al, 2014; and Van Avendonk et al., 2014). During the experiment, the instrumentation and analysis techniques were improved compared with the TAICRUST project, and more comprehensive datasets were acquired, especially for the offshore areas (McIntosh et al., 2012). The difficulty in processing such a marine dataset is to attenuate the multiples in the data (Lester et al., 2012a). In southern Taiwan, the volume of accreted crust increases from south to north. Thus, McIntosh et al. (2013) proposed that the Central Range was formed from the accreted crust. In southwest Taiwan, Lester et al. (2013) proposed a model of arc-continent collision in which the crust is in an early stage of collision and is subsequently uplifted and exhumed to the surface during collision. In south Taiwan, in the range of N19°-21.5° Eakin et al. (2014) proposed a collision model in which, prior to true arc-continent collision, blocks of hyperextended continental crust of rifted China margin were subducted and underplated into the accretionary prism along preexisting detachment surfaces. Further south of Taiwan, in the Northeastern South China Sea, the crust and mantle may also have become decoupled as a result of post-rift magmatism, likely after the South China Sea spreading (McIntosh et al., 2014). Based on the current results from the TAIGER datasets, the velocity profiles from the northern South China Sea to southern Taiwan indicate the onset of arc-continent collision.

Furthermore, a detailed study of the crustal structure in the Taiwan Strait and Fujian, west of the Taiwan orogen, could provide the initial crustal properties of Taiwan before the collision that built the mountain belt to better understand the mountain building process. Therefore, in 2010, a wide-angle onshore-offshore seismic project, the Across Taiwan Strait Explosion Experiment (ATSEE), was performed to cover the range of the connection from the Fujian province to the island of Taiwan. Additionally, collaboration with the Earthquake Administration of Fujian Province extended the 2D crustal structure from the offshore area east of Taiwan to Fujian Province (Fig. 2).

In this study, we integrated the datasets of both the crustal refracted and the reflected arrival times of air guns and explosions from TAIGER and ATSEE to model the crustal structure along three EW transects from north to south to obtain better velocity structure constraints and to determine the Moho variations in this region (Fig. 2).

2. Tectonic and geological background

The plate configuration in southeastern China involves two subduction systems, one active collision zone, and one old orogen (Fig. 1). Considering the subduction systems, the Eurasian plate (EUP) subducts to the east beneath the Philippine Sea plate (PSP) along the Manila trench in southern Taiwan, whereas in the offshore area northeast of Taiwan, the Philippine Sea plate subducts to the north under the Eurasian

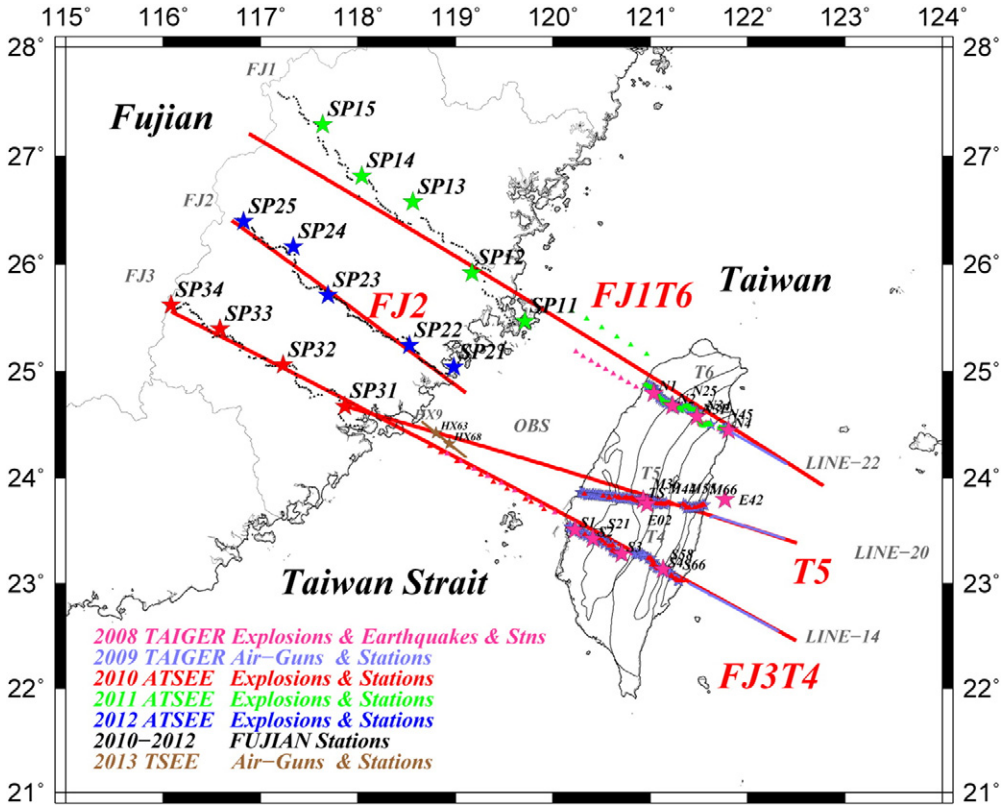

Fig. 2. The survey geometries of the TAIGER, ATSEE, and TSEE projects from 2006 to 2013 in this study. Each color represents the corresponding sources (stars) and receivers (triangles mark land stations and circles mark the OBS) deployed in the experiments of that year. The solid lines and large characters in red color show the locations of 3 projected transects. The code names are shown in the figure.

plate along the Ryukyu trench. Two mountain belts, the Wuyi-Yunkai and Taiwan orogens, have different documented tectonic collisional histories (Fig. 1). The Wuyi-Yunkai orogen, regarded as an old intraplate orogen, was created during the early Paleozoic era (e.g., Charvet, 2013), whereas the Taiwan orogen was formed by an active interplate collision since the late Cenozoic era (~6.5 Ma; Chai, 1972) (Fig. 3a and b). The Taiwan orogen was formed between two subduction systems due to the transitional continental plate of the EUP colliding with the oceanic plate of the PSP (Fig. 3b). Between these two orogens, the tectonics along the southeastern coastline of Fujian and the Taiwan Strait were related to the backarc extension owing to the ancient Pacific plate that was subducted to the west during Mesozoic era (e.g., Li, 2013) (Fig. 3a). Currently, the stress field in this region is affected not only by the northwestern movement of the PSP but also by the northern movement of the Indian plate (Zhou et al., 2001).

2.1. Evolution Models

As a result, this region has been through several stages of crustal evolution since the Paleozoic era to form the current crustal structure (e.g., Grabau, 1924; Jahn et al., 1976; Li, 2013). Here, there are 3 preferred models for the areas in Fujian, Taiwan, and southeast Taiwan.

In Fujian, the tectonic environment could be formed earlier. With the closure of the paleo-south China ocean in the Neoproterozoic (1000-900 Ma.), the convergence of the Cathaysia block and the Yangtz block began, and the subsequent collision of the Cathaysia block and the Yangtze block occurred (870 Ma.) and formed the South China continent. Owing to the worldwide breakup of the Rodinia Supercontinent (860-800 Ma.), the South China continent was separated into several microcontinents (Shu et al., 2011). During the Indosinian movement in the late-Paleozoic to early-Mesozoic, the South China continent collided with the Indian plate and the Sibumasu continent (258-243 Ma.), then experienced underplating by the paleo-Pacific plate (253-239 Ma.), and later collided with the North China continent (240-225 Ma.), mainly in the N-S direction, to produce the tectonic frame of southeast China. The geologic environment of the Fujian area was mainly created during the Yanshanian movement in the Mesozoic. The underplating of the paleo-Pacific plate was oblique and became the main role of tectonic force as an intraplate orogeny to create a large area of magmatism within the Cathaysia block in 175 Ma. Subsequently, the oblique underplating rotated by 80° to become opposite underplating to the south China continent and formed a comprehensive volcanic intrusions belt in the continental margin of east Asia in 120 Ma. (Mao et al., 2014). The metamorphic belt was thrust onto the rocks of magmatic belt along the coastline of Fujian by the opposite underplating in the Yanshanian movement in the Mesozoic (132-82 Ma.) (Chen et al., 2002). The southeast China block was pushed over the Philippine Sea by the eastward displacement of the central China block by the north-south convergence between the Indian and Eurasian Plates in the Tertiary period (Tapponnier and Molnar, 1977). In summary, it is generally believed that the current tectonics in the Fujian area were created by westward underplating of the paleo-Pacific plate with a low dipping angle and high subducting rate during the Yanshanian movement in the Mesozoic.

For the Taiwan orogeny, the mountain range was created by the oblique arc-continent collision between the Philippine Sea Plate and the Eurasian Plate ~6.5 Ma. (Chai, 1977). Taiwan is located at the junction of the Manila trench and the Ryukyu trench (Roecker et al., 1987). The Philippine Sea Plate is moving northwest with a velocity of 8.2 mm/yr based on the GPS data (Yu et al., 1997). In addition, many studies have been performed to constrain the specific portions of Taiwan. Rau and Wu (1995) resolved the images beneath the Central Range and showed that the velocities are high at the shallow depth of ~10-15 km. The high velocity in the upper crust seems to continuously extend into the lower crust, which is not appropriate for thin-skinned modeling. Ma et al. (1996) stated that the variation in the crustal

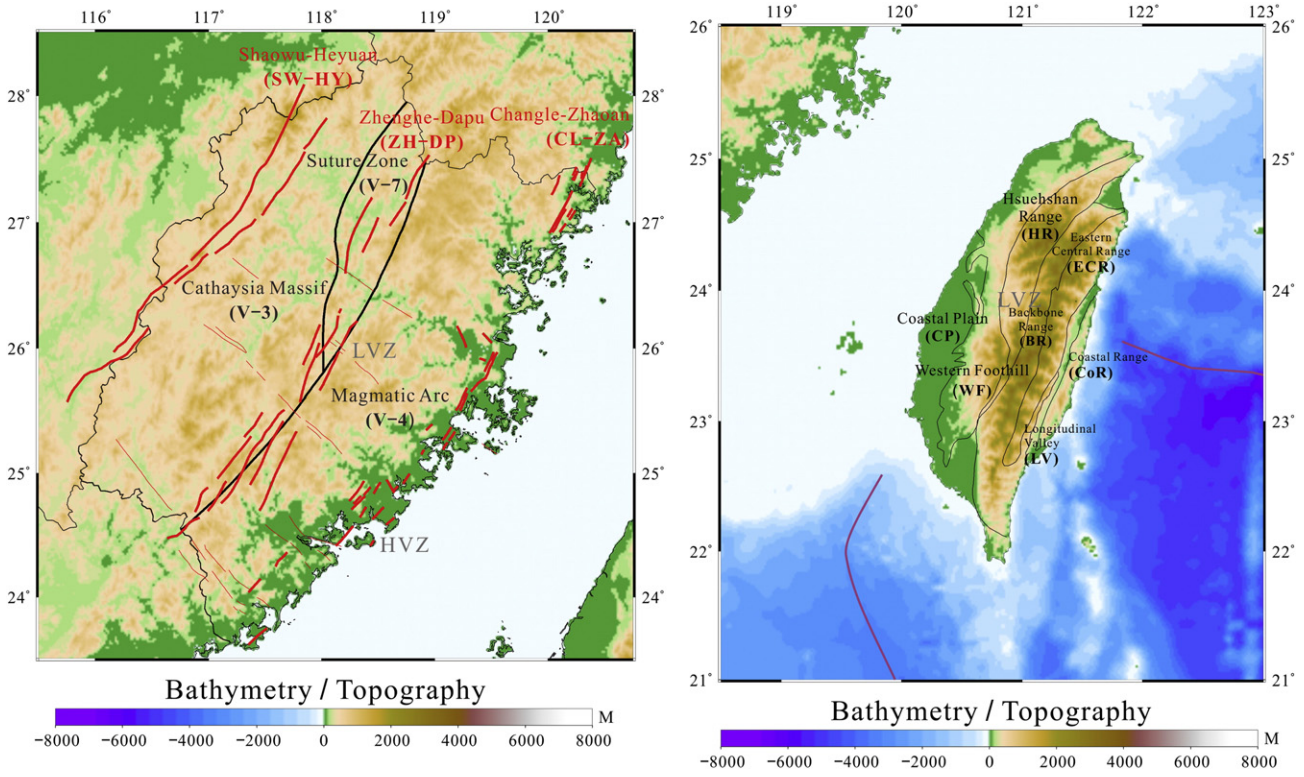

Fig. 3. The brief geological provinces of Fujian(a) and Taiwan(b). The code names from west to east are (a) V-3, Cathaysia massif; V-7, suture zone of central Fujian; V-4, magmatic arc of coastal Southeast, and (b) CP, Coastal Plain; WF, Western Foothills; HR, Hsuehshan Range; BR, Backbone Range; ECR, Eastern Central Range; LV, Longitudinal Valley; CoR, Coastal Range. The red color in (a) represents the major fault zones in Fujian. The purple solid lines in (b) represent the locations of trenches.

Table 1
The data volume from this study. There are 40 shots, 2 earthquakes, 1950 stations, and 10 survey lines involved. In total, 15,612 were picked for modeling, which are from 5815, 840, 2105, and 7392 selections for survey lines FJ1T6, FJ2, T5, and FJ3T4, respectively. The red characters are the independent shots used in each modeling process.

Data Volume of FJ1T6

Year	DataSet	ShotPoint	Picks	Total
2008TAIGER_TW	Explosion	N1	681	681
2008TAIGER_TW	Explosion	N2	431	1112
2008TAIGER_TW	Explosion	N3	751	1863
2008TAIGER_TW	Explosion	N3P	432	2295
2008TAIGER_TW	Explosion	N4	434	2779
2009TAIGER_TW	Onshore-Offshore	N25	1315	4044
2009TAIGER_TW	Onshore-Offshore	N34	625	4669
2009TAIGER_TW	Onshore-Offshore	N45	375	5044
2011ATSEE_FJ	Across Taiwan-Strait	SP11	75	5119
2011ATSEE_FJ	Explosion	SP11	114	5233
2011ATSEE_FJ	Explosion	SP12	177	5410
2011ATSEE_FJ	Explosion	SP13	158	5568
2011ATSEE_FJ	Explosion	SP14	127	5695
2011ATSEE_FJ	Explosion	SP15	120	5815
Total			5815	
Pg Phase L1			**132**	132
Pg Phase L2			**559**	691
Pg Phase L3			**998**	1689
Pg Phase L4			**2573**	4262
Pg Phase L5			**320**	4582
Pn Phase L5(UM)			**346**	4928
PcP1 Phase L4			**217**	5145
PcP2 Phase L5			**200**	5345
PmP PhaseL5(UM)			**470**	5815
Total			**5815**	

Data Volume of FJ2

Year	DataSet	ShotPoint	Picks	Total
2012ATSEE_FJ	Explosion	SP21	107	107
2012ATSEE_FJ	Explosion	SP22	171	278
2012ATSEE_FJ	Explosion	SP23	201	479
2012ATSEE_FJ	Explosion	SP24	162	641
2012ATSEE_FJ	Explosion	SP25	199	840
Total			840	
Pg Phase L1			**159**	159
Pg Phase L2			**164**	323
Pg Phase L3			**3**	326
Pn Phase L5(UM)			**106**	432
PcP1 Phase L3			**205**	637
PcP2 Phase L4			**140**	777
PmP PhaseL5(UM)			**63**	840
Total			**840**	

Data Volume of T5

Year	DataSet	ShotPoint	Picks	Total
2006TAIGERTest	DILI Test Shot	DILI Test Shot	143	143
2008TAIGER	Earthquake	EQ#02	204	347
2008TAIGER	Earthquake	EQ#42	113	460
2008TAIGER	Onshore-Offshore	M36	138	598
2008TAIGER	Onshore-Offshore	M44	650	1248
2008TAIGER	Onshore-Offshore	M55	488	1736
2008TAIGER	Onshore-Offshore	M66	249	1985
2008TAIGER	Onshore-Offshore	Lin07#1179	47	2032
2010ATSEE	Across Taiwan-Strait	SP31	73	2105
Total			2105	
Pg Phase L1			**189**	189
Pg Phase L2			**308**	497
Pg Phase L3			**598**	1095
Pg Phase L4			**563**	1658
Pg Phase L5			**113**	1771
Pn Phase L5(UM)			**334**	2105
Total			**2105**	

Data Volume of FJ3T4

Year	DataSet	ShotPoint	Picks	Total
2008TAIGER_TW	Explosion	S1	1121	1121
2008TAIGER_TW	Explosion	S2	787	1908
2008TAIGER_TW	Explosion	S3	670	2578
2008TAIGER_TW	Explosion	S4	788	3366
2008TAIGER_TW	Across Taiwan-Strait	S1	9	3375
2009TAIGER_TW	Onshore-Offshore	S21	110	3485
2009TAIGER_TW	Onshore-Offshore	S58	1489	4974
2009TAIGER_TW	Onshore-Offshore	S66	1243	6217
2010ATSEE_FJ	Explosion	SP31	139	6356
2010ATSEE_FJ	Explosion	SP32	135	6491
2010ATSEE_FJ	Explosion	SP33	176	6667
2010ATSEE_FJ	Explosion	SP34	143	6810
2010ATSEE_FJ	Across Taiwan-Strait	SP31	56	6866
2013TSEE_FJ	Onshore-Offshore	HX63	294	7160
2013TSEE_FJ	Onshore-Offshore	HX68	232	7392
Total			7392	
Pg Phase L1			**554**	554
Pg Phase L2			**2051**	2605
Pg Phase L3			**1178**	3783
Pg Phase L4			**946**	4729
Pg Phase L5			**150**	4879
Pn Phase L5(UM)			**1204**	6083
PcP2 Phase L3			**377**	6460
PcP3 Phase L4			**428**	6888
PmPPhase L5(UM)			**504**	7392
Total			**7392**	

thickness in Taiwan is in the range of ~ 30-40 km. Kim et al. (2005) further mentioned that the crustal thicknesses are 35 km, 50-55 km, and 25 km beneath the Western Foothills, Central Range, and Coastal Range, respectively. Wu et al. (2007) found that the deepest point of the Moho boundary in Taiwan is 60 km if the velocity contour of 7.8 km/sec is taken to be the reference line. Kuo-Chen et al. (2012b) proposed that it is hot and dry in the mid-lower crust beneath the Central Range based on the low Vp/Vs ratio of ~1.55 and high resistivity of ~500 Ohm-m, indicating an anhydrous condition. In summary, the preferred evolution model for Taiwan could be a subduction zone in southern Taiwan with the upper mantle high velocity anomaly along the trend of Taiwan, and a stoppage of eastward subduction toward the north in central Taiwan based on the lack of associated seismicity in central Taiwan and the disappearance of the organized high velocity anomaly under northern Taiwan (Kuo-Chen et al., 2012a).

In southern Taiwan, the continental crust is extended, underthrusted to ~15 km below the accretionary prism, and subducted beneath the Manila trench (McIntosh et al., 2013). In southwest Taiwan,

a distal margin crust that subducted beneath an accretionary wedge and contained a highly extended continental crust with interspersed volcanic bodies was found (Lester et al., 2013). Further south of Taiwan, Eakin et al. (2014) found more evidence of the ~6-km-thick oceanic crust, ~12-km-thick extended continental crust, and ~15-km-thick extended continental crust in the transects that are perpendicular to the Manila trench and located at N19°, N20.5° and N21.5°, respectively. Much further south of Taiwan, the crust in the Northeastern South China Sea shows the deformation history of necking and subsequent breakup (McIntosh et al., 2014). In summary, based on the current results from the TAIGER datasets and the velocity profiles from the northern South China Sea to southern Taiwan, a preferred model was proposed that consisted of an extended crust southwest of Taiwan undergoing incipient arc-continent collision and a forearc accreted in the north, forming the Central Range during the collision.

2.2. Faults

From the Wuyi-Yunkai orogeny to the Taiwan orogeny, there are some important boundaries. In Fujian, this area developed a series of faults and a series of undulate hills. There are 3 major NNE oriented faults, the Changle-Zhaoan fault zone (CL-ZA), the Zhenghe-Dapu fault zone (ZH-DP), and the Shaowu-Heyuan fault zone (SW-HY) (Fig. 3a). The studies from chronology and geology stated that the Zhenghe-Dapu fault zone is an ancient suture zone, which separates the Early Paleozoic fold belt to the west from the Late Mesozoic magmatic belt to the east (Li, 2013). There are also several NNW oriented faults, which are perpendicular to the NNE main fault zones.

After the breakup of the Rodinia Supercontinent, the Cathaysia block was also separated into 2 microcontinents as the western and eastern Cathaysia blocks, at least before the Indosinian (240 Ma.) or even Caledonian (450 Ma.). The 2 microcontinents collided with each other again until the Yanshanian event in the Mesozoic (160 Ma.) (Xu et al., 2007). Under this framework in southeast China, the suture zone between the Yangtz and Cathaysia blocks is the Shaoxing-Jiangshan-Pingxiang fault, which has a length of ~1200 km, and the suture zone that separated the Cathaysia block into 2 microcontinents is the Zhenghe-Dapu fault, which has a length of ~800 km (Cai et al., 2015). In contrast to the geodynamic mechanism of the Jiangnan orogeny, the Wuyi-Yunkai orogeny showed intraplate evolution that was caused by the underplating of the paleo-Pacific plate. Cai et al. (2015) proposed a model in which the Zhenghe-Dapu fault zone is a suture zone between the western and eastern Cathaysia blocks and consists of a rifted basin filled with chaotic sedimentation along with bimodal igneous rocks in central Fujian province in southeastern China. With the same evolution mechanism, the westernmost boundary within the Fujian area is the Shaowu-Heyuan fault. The Changle-Nanao fault (same as the Changle-Zhaoan fault mentioned above) divided eastern Fujian into a Cretaceous magmatic belt to the west and the Pingtan-Dongshan metamorphic belt to the east by the opposite underplating of the paleo-Pacific plate after 120 Ma (Chen et al., 2002).

In Taiwan, the suture zone is the Longitudinal Valley, which is between the Central Range in the west and the Coastal Range in the east

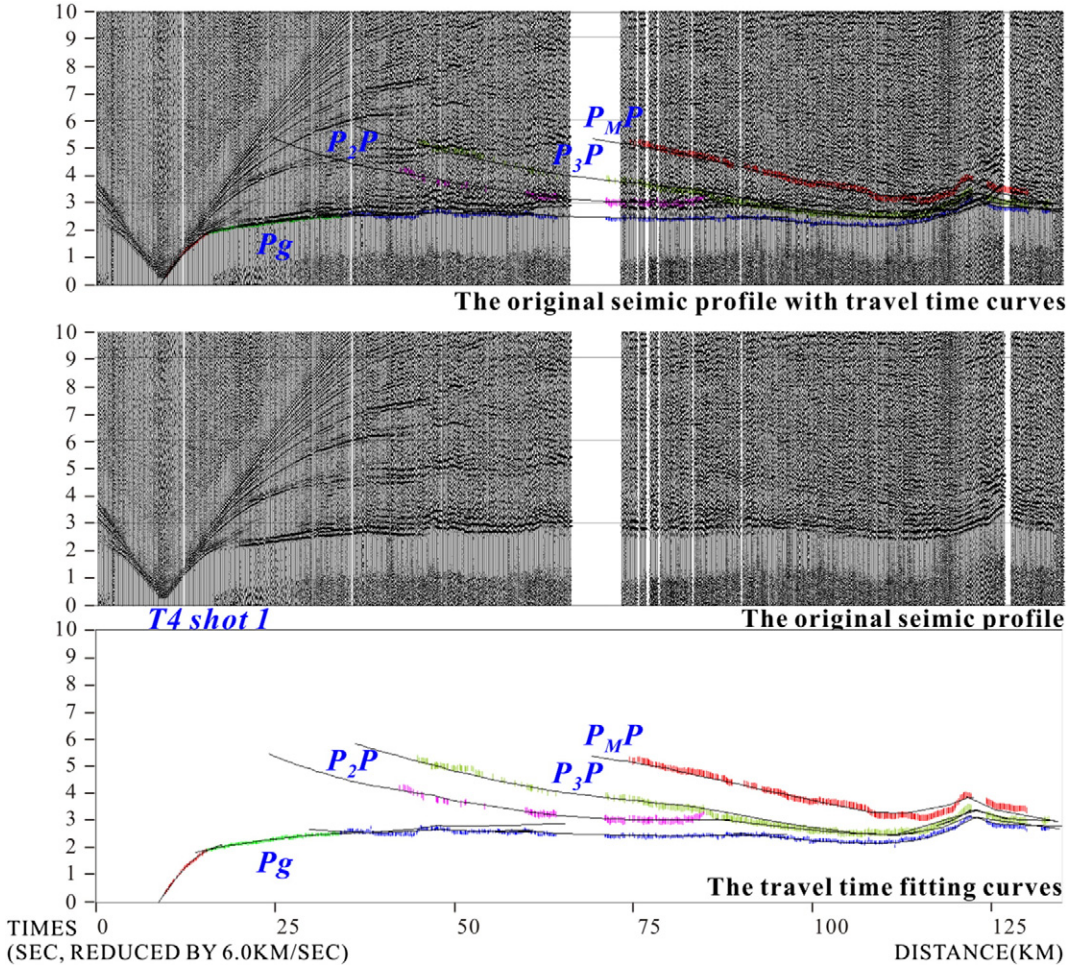

Fig. 4. Seismic data profile of shot 1 along survey line T4. It shows the Pg, PcP, and PmP phases. The upper panel shows the data profile with the predicted and observed travel time curves and interpreted phases. The middle panel shows the data profile. The lower panel shows the predicted and observed travel time curves and interpreted phases. The reflections can be identified in the profile and fitted with predicted travel time curves.

(Ho, 1999). Van Avendonk et al. (2014) proposed that the upper crustal rocks and sediments from the Eurasian Plate are underthrusting the Central Range to ~ 25 km depth with a velocity of 5.5 km/sec, and the root of a mafic average composition is found with a velocity between 6.0 -7.5 km/sec in middle and eastern Taiwan.

2.3. Geological Units

The tectonic units in Fujian can be defined in three large units from east to west as follows (Fig. 3a): (1) Jurassic-Cretaceous magmatic arc of the coastal Southeast (V-4), composed of a volcanic arc, basin, and magmatic complex rocks; (2) suture zone of central Fujian (V-7), composed of the Paleozoic pelagic sedimentary rocks, basaltic debris, and ophiolite mélange; and (3) Cathaysia massif (V-3), the Paleozoic inter- and back-arc basin, and rift basin (Li, 2013).

In contrast, the geologic/tectonic units in Taiwan are defined from east to west as follows (Fig. 3b): (1) the Coastal Range (CoR), the compressed Luzon Arc and its forearc basin; (2) the Longitudinal Valley (LV), the suture between the Eurasian and Philippine Sea plates that separates the CoR from (3) the pre-Tertiary basement of the continental margin of the Eastern Central Range (ECR); (4) the Backbone Range (BR), composed of Miocene to Eocene slates; (5) the Hsuehshan Range (HR), built mostly from the Eocene and Oligocene continental shelf sediments from the west; (6) the Western Foothills (WF), composed of accreted and deformed sediments in the foreland basin; and (7) the Coastal Plain (CP), the present-day foreland basin (Ho, 1986).

3. Data

The TAIGER (2008-2009) project was a joint USA-Taiwan program in collaboration with Japanese and French scientists. One of the important field experiments in this project was the active source experiment, which began with a test shot of 500 kg dynamite in Nantou County in 2006. Later, for the onshore active sources, 10 shots were executed in 2008 (February to March) within the range of 750 ~ 3000 kg of dynamite, and each of the 5 shots were distributed uniformly with a spacing of 20-30 km along the 99-km and 133-km survey lines in northern and southern Taiwan. In addition, for the offshore active sources, 2 legs of 70 air gun ship tracks were executed in 2009 (May to July) with 6,000 inches^3 shots from the combination of 4 air-guns offshore of Taiwan. The spacing between the air gun shots were within the range of 50-150 m, which depends on the speed of the ship. For the deployment of the land stations, there were 5 linear arrays with an average spacing of 200 m during the land explosions in 2008, and there were 4 linear arrays with an average spacing of 2 km during the marine air-gun shots in 2009 (Okaya et al., 2009). Subsequently, the TAIGER and ATSEE (2010-2012) projects were performed, which involved collaboration between scientists in Taiwan and Fujian for the purpose of understanding the crustal structure beneath the Taiwan Strait and Fujian province. During the experiment, there were 18 explosions with a spacing of 50-70 km and 8 linear arrays of receivers with an average spacing of 2 km. In addition, many experiments are planned for this area to increase the database and improve the resolution of the crustal structure beneath the Taiwan Strait, such as the ongoing main experiment: the TSEE project (Taiwan Strait Explosion Experiment) from 2013 to 2017. In summary, we integrated the data sets from different experiments (2008, 2009, 2010-2012, and 2013) and extracted the data for the east-west orientation to determine the velocity transects. These data can be combined and grouped into 3 transects in the Northern, Middle, and Southern areas for analysis (Fig. 2 and Table 1).

Because of the dense spacing of the seismic arrays, the Pg phases are the first arrivals and are very clear and easy to identify at distances of

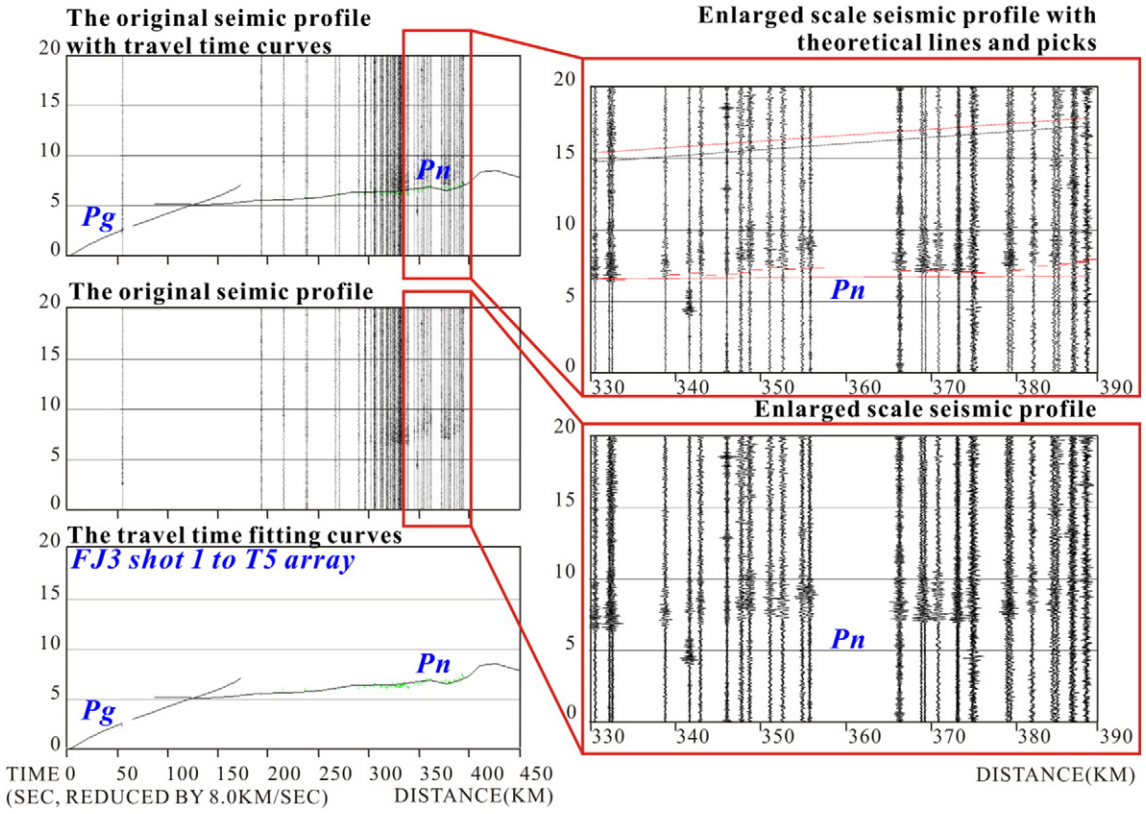

Fig. 5. Seismic data profile consists of signals from shot1 on survey line FJ3 to the receiver array along T5. It shows the Pg and Pn phases. The upper panel shows data profile with predicted and observed travel time curves and interpreted phases. The middle panel shows the data profile. The lower panel shows the predicted and observed travel time curves and interpreted phases. On the right are the enlarged profiles for the Pn arrivals that were received in Taiwan. The clear Pn picks can be identified from the Fujian coast to a distance as far as 390 km from the eastern coast of Taiwan.

less than 100 km. However, the Pn phases, i.e., the arrivals of head wave that travels along Moho boundary, appeared as the first arrivals instead of the Pg phases at distances greater than the cross-over distance of ~150 km in the Taiwan Strait direction (to the west) and ~55 km in the Pacific Ocean direction (to the east). The crustal reflections can be recognized around the distance of ~100 km without any other advanced processing, which indicates that the impedances are large enough to observe in the original shot gathers. For instance, in Fig. 4, the shot gather from explosion (S1) along the T4 survey line shows the Pg, PcP, and PmP phases. In Fig. 5, the shot gather from explosion SP31 shows that the Pn phase traveled across the Taiwan Strait and reached as far as 390 km along the eastern coast of Taiwan. Additionally, to distinguish the reflections from the Moho, the mid-crust, and multiples in the strong signals, we applied NMO correction to see the hyperbolic characteristics and continuity of the strong signals and plot theoretical curves on the figure showing the shot gathers as guidance for picking out the continuous signals as reflections. Because the normal move-out (NMO) correction and the assistant theoretical travel time curves were used with values in a reasonable range, the strong hyperbolic curves with NMO values in the ranges for specific reflectors, such as 5.5-6.0 km/sec and 10-20 km for the upper-mid reflector, 6.0-6.5 km/sec and 20-30 km for the mid-lower reflector, and 6.5-7.5 km/sec and 30-40 km for the Moho boundary, should represent the corresponding reflection signals well (Fig. 4).

Table 1 shows the number of picks used, and Fig. 6 shows the travel time curves of picks for three transects. The quality of these picks is as good as the continuity of the travel time curves. In total, 40 shots, 2 earthquakes, and approximately 1,950 stations were used, and 15,612 picks of P-wave arrivals were picked (5,815, 7,392, 2,105, and 840 picks for the Northern transect, Southern transect, eastern part of the Middle transect, and western part of the Middle transect, respectively). For the Middle transect, the FJ2 and T5 survey lines were modeled separately because their cut angle is too large to make reasonable travel time reductions to allow projection in one transect. These datasets were provided by the signals from the crust and mantle as Pg, PmP, Pn, and intermediate-crustal reflection phases.

Table 2 shows the data processing flowchart of this study. The purpose of the first step is to pick out reliable arrival times from the raw data after some steps. The standard parameters used throughout this study have the following values, which help determine the optimal parameters for special cases. These parameters include cutting the data

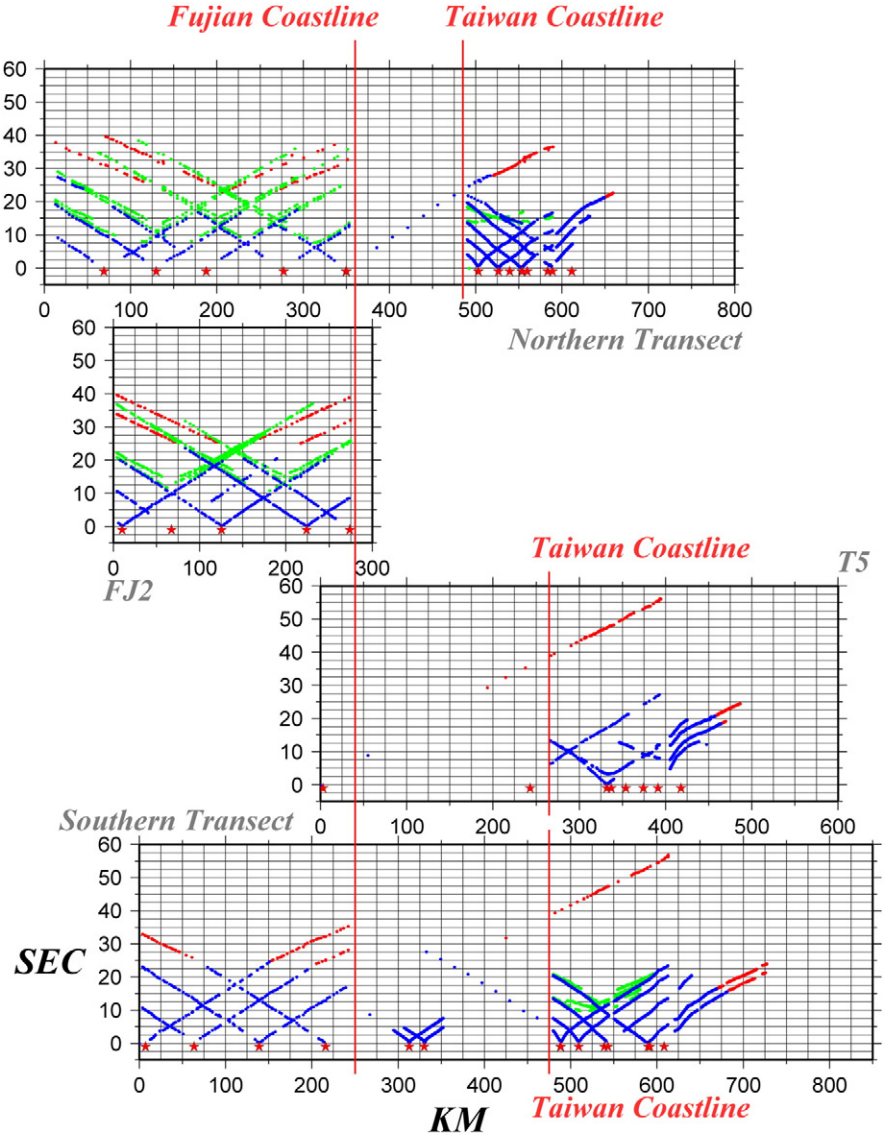

Fig. 6. The data picks used in this study. In total, 15,612 picks were used. The travel time curves shows the good data quality. The plots were aligned along Fujian coast for understanding. The red vertical solid lines mark the locations of coastlines. Blue Dots: Refractions. Red Dots: Head Waves. Green Dots: Reflections.

Table 2
The routine data processing flowchart representing this study. There are 5 main steps in the flowchart. Details of each steps will be described in the text. The step of "Pre-Data Processing" is described in the "Data" section. The other 4 steps are described in the section of "Methodology".

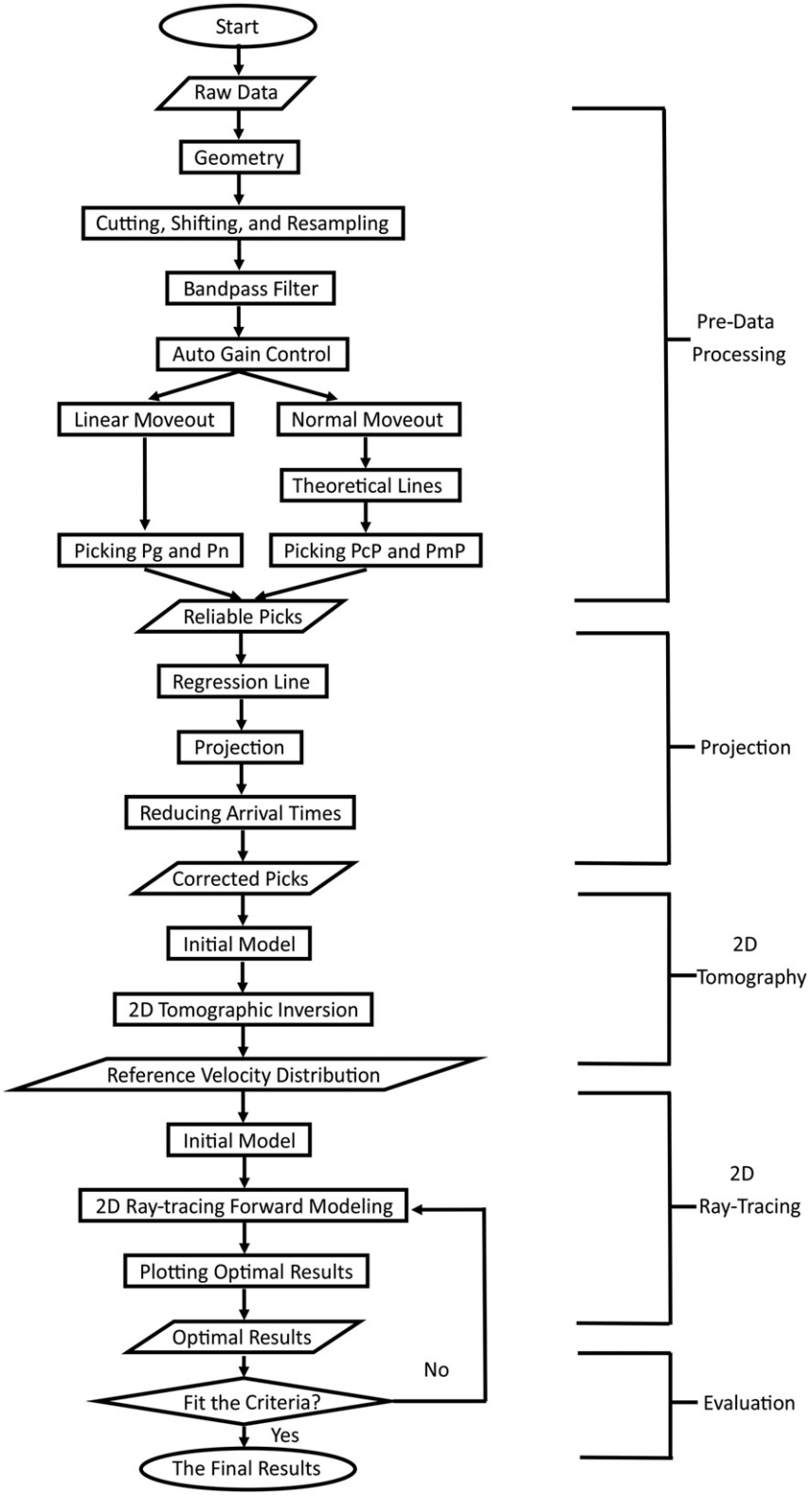

into 5 minute sections, shifting the source time to 0, using a band-pass filter of 3-10 Hz, applying an Auto Gain Control of 3 seconds, correcting with Linear Moveouts of 6.0 and 8.0 km/sec for the Pg and Pn phases, respectively, or with Normal Moveout for reflections, and then drawing theoretical lines as a guide for the eye picking. Examples are shown in Figs. 4 and 5; they were derived using the steps mentioned above but

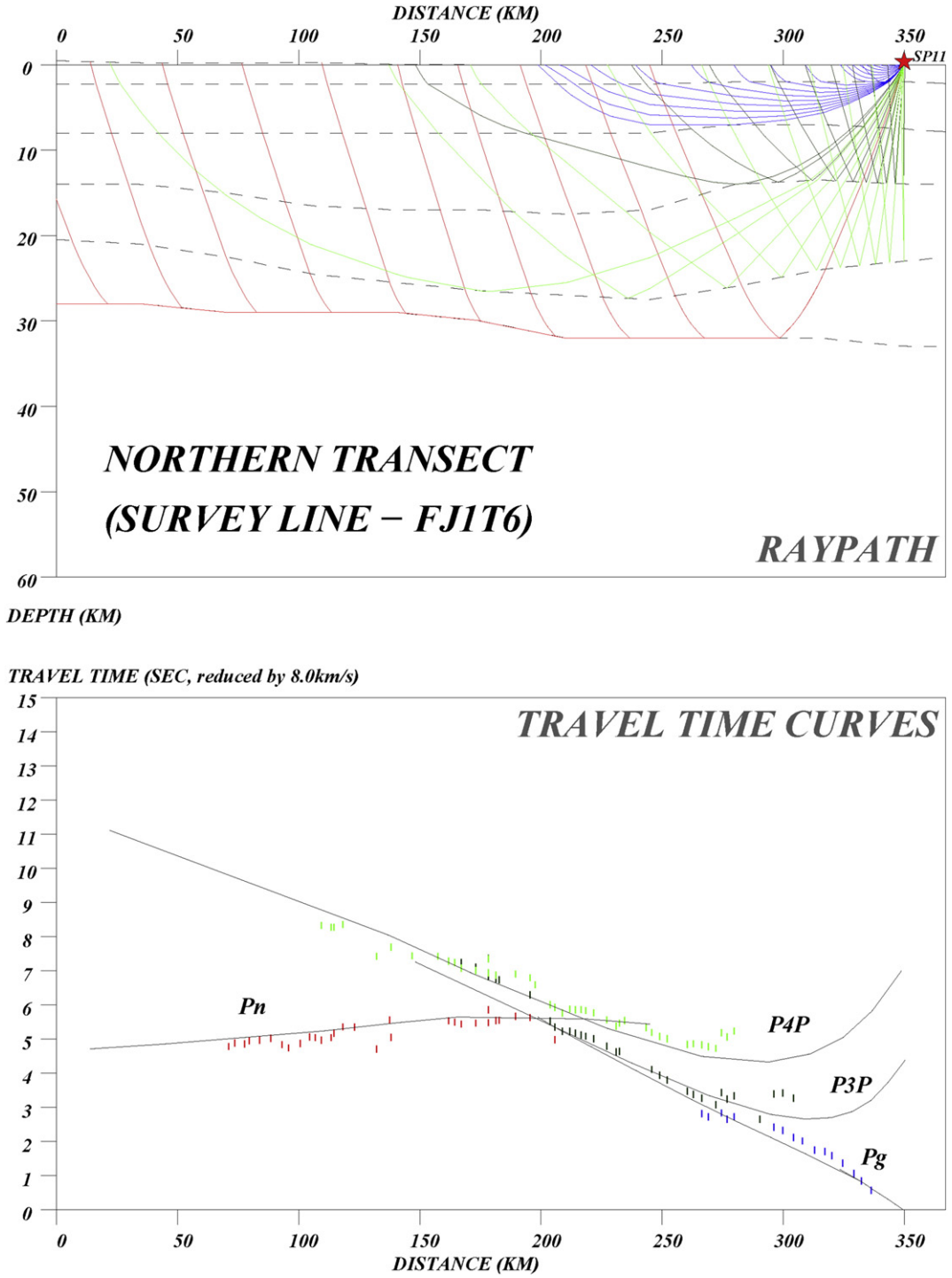

Fig. 7. An example showing forward modeling by the ray-tracing method using shot 1 along survey line FJ1. The blue, black, green, and red colors represent the Pg, P3P, P4P, and Pn phases, respectively. The solid lines in the upper and lower panels are the theoretical ray paths and travel time curves, respectively. In addition, the dots in the lower panel are the observed travel time picks. For cautious modeling, the velocity structure can be constructed by grouping the observed arrivals into corresponding phases. Then, the velocity model will be reliable if predicted travel time curves can fit all grouped phases of observed travel time curves well.

with different reduced velocities and different receiver spacing (6.0 km/sec and 200 m for Figs. 4, and 8.0 km/sec and 2 km on average for Fig. 5) such that they look slightly different.

4. Methodology

The strategy of ray-tracing modeling uses the layer-stripping method (Zelt and Forsyth, 1994), and the topography is taken account and parameterized into the initial model. The forward modeling starts with fitting the predicted and observed first arrival times. Then, we model the reflections, which focuses on locating the depth of the reflectors and treating the velocity distribution derived from first arrival times as the background values. The forward modeling was performed from top to bottom reflectors and resulted in an optimal model. The average velocity and depth variation of certain reflectors are controlled in a small and reasonable range, which corresponds to the NMO results showing strong and continuous reflections of that reflector. In contrast, with the damped least-square method, a better model can be derived

automatically through calculation from an initial solution toward a closer solution within 5 iterations, in our experience. The statistic parameters for assessment can be improved efficiently in this way, but care needs to be taken to restrict the improvement to within a reasonable range. Because of the calculation, the improvements may be trapped in some specific areas with larger differences in the model. Instead of treating the closer solution as the final answer when the convergence is difficult to reach or the closer solution is an unusual extreme, the

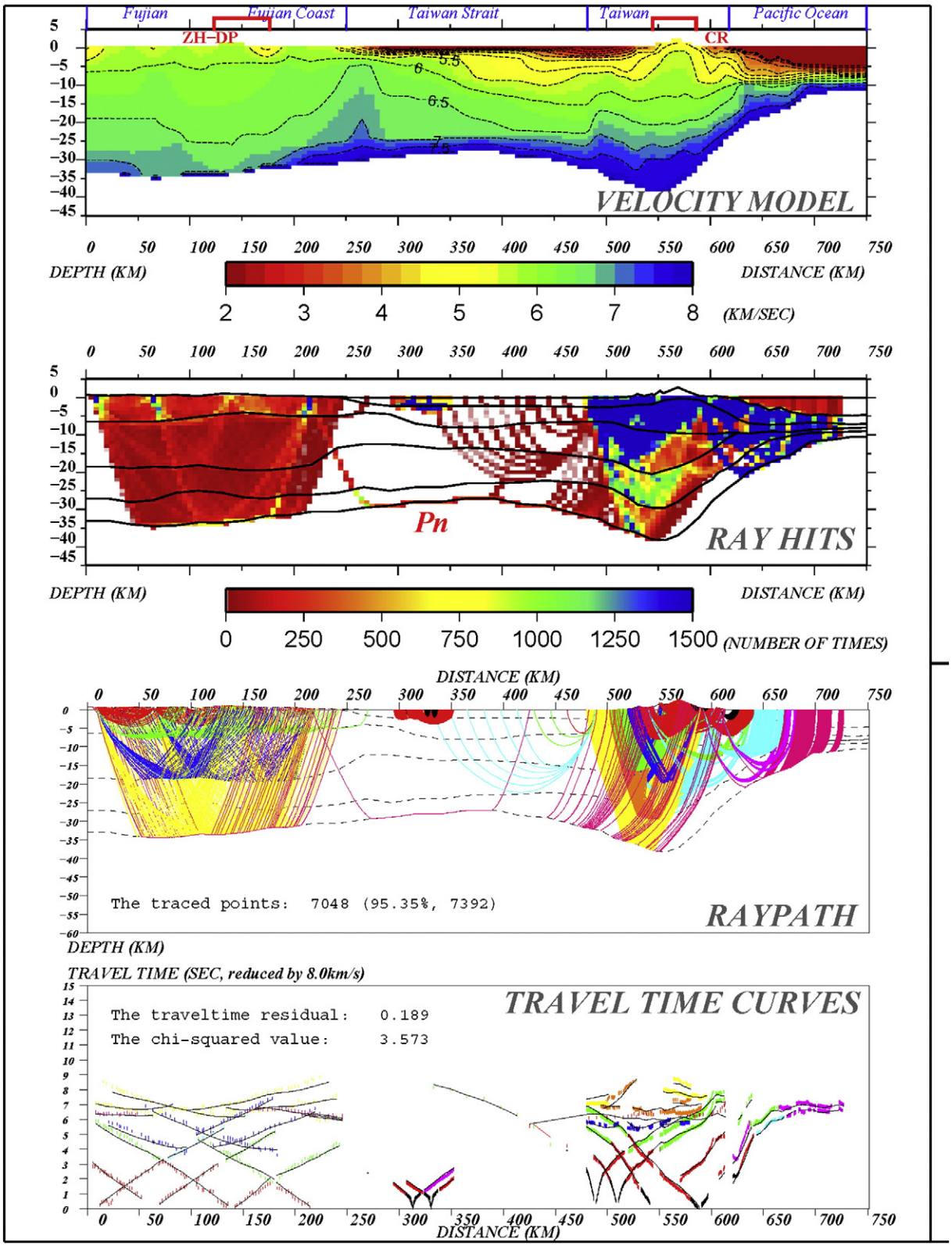

Fig. 8. The final result of Southern Transect, FJ3T4. The upper panel shows the final velocity model. The second panel is the ray hits. The third panel shows the theoretical ray path. The bottom panel is fitting curves between predicted and observed travel times. The ray coverage is good beneath both Fujian and Taiwan. Ray coverage is not good beneath the Taiwan Strait. However, the Pn phase across the Taiwan Strait provides some constraints on the lower crust.

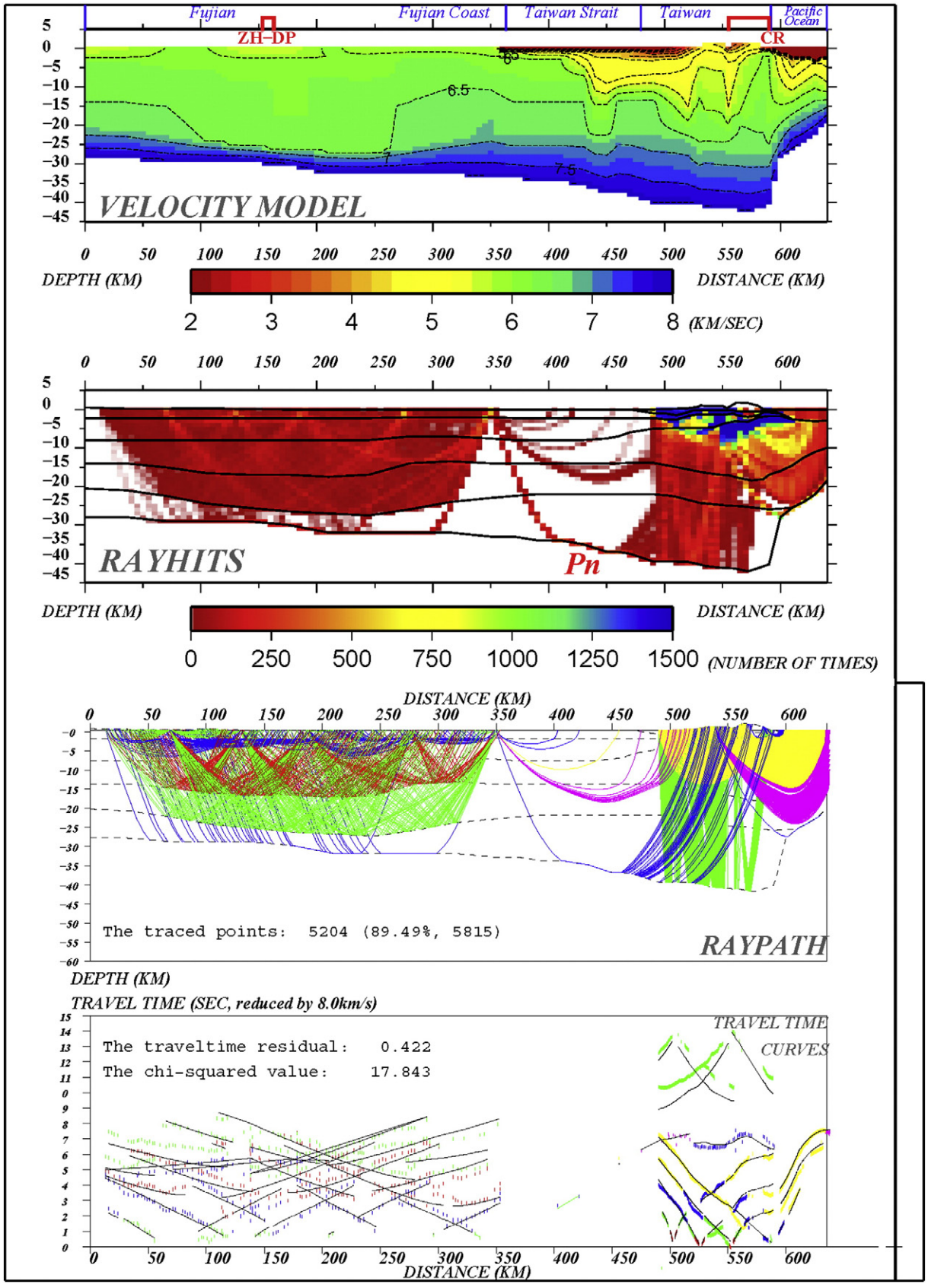

Fig. 9. The final result of the Northern Transect, FJ1T6. The upper panel shows the final velocity model. The second panel shows the ray hits. The third panel shows the theoretical ray paths. The bottom panel shows the fitting curves between predicted and observed travel times. The ray coverage is good beneath both Fujian and Taiwan. In addition, the Pn phase and reflections provide constraints on the mid – lower crust.

damped least-square method can alternatively be used to show where and how we can improve the fitting curves in the parts that are difficult to discover. In general, the statistical parameters of RMS < 0.2, chi-square ~ 2, ray path with a wider range, and ray density with a higher value indicate that the derived model is a good solution for the final result. However, a model with values that fall in the range of these criteria is not easy to derive. As an alternative, values that are close to the criteria are also an acceptable solution for the final result.

As shown in the flowchart (Table 2), the details of the routine process will be performed as follows:

1) With proper data processing as described in the data section, reliable arrival times can be picked and the reference line for projection can be made based on the survey geometry.
2) After the reference line for each transect is chosen, the picked arrival times are reduced reasonably according to the source-receiver distances after the projection.
3) After the picked arrival times are corrected through projection, we immediately run the 2D tomographic inversion using Hole's code (Hole, 1992) as an initial velocity model for the forward modeling. During this 2D tomographic inversion, the built geometry and corrected arrivals can be verified again by deriving the velocity distribution without severe errors.
4) After the velocity distribution is derived, we can begin 2D forward modeling using the ray-tracing method (Zelt and Smith, 1992). For example, as shown in Fig. 7, the phases of the observed travel time curves can be verified in detail with a given velocity model. If the predicted travel time curves do not fit the observed travel time curves, we adjust the given model until they fit well and all of the phases correspond to each other well. Such a model can be treated as the final result of this modeling.
5) In the last step, the statistical numbers of RMS, chi-square, ray path, and ray density from the final result are used to determine whether the final velocity model is acceptable or not.

Through this procedure, the given model can be adjusted iteratively according to the static numbers to improve the model and its reliability. However, there is one exception: the final T5 model is abnormal and has difficulty converging due to the presence of a velocity reversal area, LVZ. In this case, the forward modeling was performed with 4 different initial models for testing, such as a gradient model with velocity increasing with depth, an LVZ model with a small anomaly, an LVZ model with an extreme anomaly, and an LVZ model with a moderate anomaly. The last of these models fits the observed data best.

5. Results

For all of the modeling in this study, the velocities beneath the Moho boundary in the upper mantle are fixed at 8.0 km/sec and are masked in crustal velocity models in the upper panel. The velocity gap changes between the lower crust and the upper mantle are held at least in the range from 0.25-0.5 km/sec for different areas. For the implementation of head waves in Zelt's modeling program, the ray paths act as waves that go along the boundary, while the true Pn waves should go along the boundary and within a small depth below the Moho boundary in the shallowest portion. However, both of them arrived at the receivers after the crossover distance as the first arrivals, which are the same from the point of view of the travel time analysis. In addition, the above mentioned points are shown in Figs. 8-10.

The modeling of the Southern transect (Fig. 8) is derived by using the combined data sets of survey lines FJ3 and T4 from the TAIGER and ATSEE projects. In total, 13 shots (S1-S4, FJ31-FJ34, S21, S58, S66, HX63, and HX68) were used and approximately 95.35% (7048/7392) of picks were traced. The statistical parameters are 0.189 for RMS and 3.573 for chi-square. The length of the final model is 750 km and the ray can cover distances as long as 728 km. From the second panel showing the ray density, the ray coverage is good beneath both the Taiwan and Fujian areas, but it is not good beneath the Taiwan Strait. There are only a few rays for Pn phase that went through the crust beneath the Taiwan Strait. Although few Pn rays passed through the Taiwan Strait, the velocities are well-constrained along its ray path because the thickness of the crust beneath the Taiwan Strait is already as shallow as possible, and the controls are good beneath both Fujian and Taiwan. The trade-off relationship between velocity and depth shows that the velocity has to decrease as the depth decreases when the travel time is fixed. Therefore, under this condition, the velocity in the lower crust beneath Fujian coastline needs to increase to fit the observed curve of the Pn phase with early arrival times unless the crustal thickness can abruptly become 4 km smaller to allow the Pn to arrive 0.5 seconds earlier. In other words, the depth of the Moho and the velocities within the lower crust have constraints beneath the Taiwan Strait. The velocity structures in the upper and middle crusts may be improved with dense ray coverage in the future. In addition, this situation is the same as that in the Northern and Middle transects in the areas beneath the Taiwan Strait. From the velocity distribution, there is a low velocity zone (LVZ) that extends from the middle crust to the lower crust with a velocity of 6.0 km/sec beneath the Zhenghe-Dapu fault zone (ZHDP) of central Fujian, and a high velocity zone (HVZ) exists in the lower crust with a velocity of 7.0 km/sec beneath the Fujian coastline. Because of the coarser receiver spacing, there are fewer rays beneath Fujian than beneath Taiwan. However, the velocities can still be constrained to a certain degree based on the PcP, PmP, and Pn phases for the middle and lower crusts beneath central Fujian. Relatively high- and low-velocity materials occur in the upper and lower crusts, respectively, beneath the mountain belt of Taiwan. The variations of the Moho boundary from Fujian to the east coast of Taiwan change dramatically as follows: ~30 km deep in west Fujian, gradually deepening toward central Fujian (~35 km), becoming shallower in the Taiwan Strait (~28 km), deepening again toward the mountain belt of Taiwan (~40 km) and becoming much shallower toward the Pacific Ocean (~10 km).

In the Northern transect (Fig. 9), the result is derived by modeling with the combined dataset of the FJ1 and T6 survey lines from the TAIGER and ATSEE projects. In total, 13 shots (N1-N4, N3P, FJ11-FJ15, SL25, SL34, and SL45) were used and approximately 89.49% (5204/5815) of picks were traced. The statistical parameters are 0.422 for RMS and 17.843 for chi-square. The length of the final model is 700 km, and the ray can covers the range as far as 655 km. From the second panel of ray density, the main pattern of coverage is the same as that in the Southern transect. The structure of the lower crust beneath the Taiwan Strait is also constrained by the Pn phase. However, the difference compared with the Southern transect beneath the Taiwan Strait is that the low-velocity materials do not extend to the lower crust because the travel time curves can be fit to each other without introducing large differences in the lateral velocity variations in the lower crust and at the Moho boundary. From the velocity distribution, the low-velocity materials beneath Taiwan do not extend to the lower crust. A LVZ beneath central Fujian extended to the lower crust with a velocity of 6.0 km/sec, and an HVZ beneath the coastline of Fujian had a gentle change in the lower crust with a velocity of 7.0 km/sec. In this transect, the Moho gradually deepens from west Fujian to the east coast of Taiwan, which is ~28 km to the west of Fujian and ~42 km from the eastern coast of Taiwan (the deepest Moho in this transect).

In the Middle transect (Fig. 10), the results are derived by modeling the datasets from the FJ2 and T5 survey lines separately because their cut-off angle is too large to integrate them using travel time reduction. However, the results are placed together for convenience. In total, 14 shots (5 for FJ2 as SP21-SP25 and 9 for T5 as SP31, Line07#1179, DILI, Line20-M36, -M44, -M55, -M66, EQ#02, and EQ#42) were used in the Middle transect. We used two earthquakes as sources for modeling because there were not enough ray paths due to only one test shot performing in 2006 in Taiwan. Van Avendonk et al. (2014) showed that the resolution is greatly improved by using earthquakes. For the

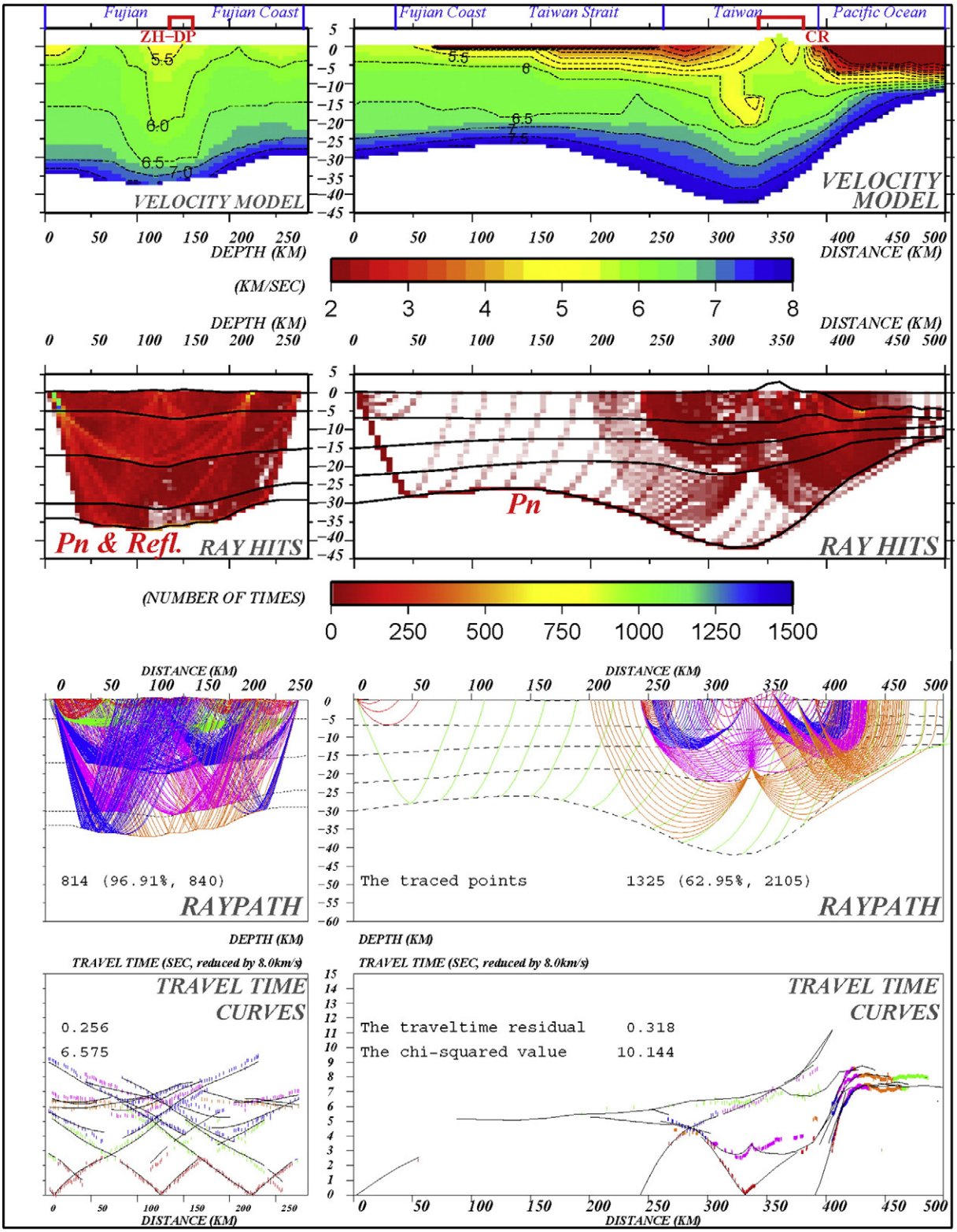

Fig. 10. The final result of the Middle Transect, FJ2 and T5. The upper panel shows the final velocity model. The second panel shows the ray hits. The third panel shows the theoretical ray paths. The bottom panel shows fitting curves between predicted and observed travel times. The modeling processes were run independently due to the cut angle between the survey lines FJ2 and T5. The mid-lower crust beneath Fujian is constrained by the PcP and Pn phases. The mid-lower crust beneath Taiwan is constrained by the Pn phase and earthquake signals.

western part of the Middle transect, FJ2, approximately 96.91% (814/840) of the picks had been traced. The statistic parameters are 0.256 for RMS and 6.575 for chi-square. The length of the final model is 300 km, and the ray can cover the range as far as 274 km. As shown in the second ray density panel, the coverage is good at depths shallower than 20 km, which provides some constraints for the lower crust via reflections and Pn phases. In the middle of the western part of the Middle transect, there is an LVZ, which is revealed by the reflections extended to the mid-lower crust with a velocity of 5.5 km/sec in central Fujian. For the eastern part of the Middle transect, T5, approximately 62.95%

(1325/2105) of picks were traced. The statistical parameters are 0.318 for RMS and 10.144 for chi-square. The length of the final model is 500 km, and the ray can cover distances as long as 486 km. Based on the second ray density panel, the coverage is good beneath Taiwan at depths shallower than 20 km, and the lower crust is constrained based on the coverage of the Pn phase from the structures under both Taiwan and the Taiwan Strait and the coverage from the earthquake signals from the structures beneath Taiwan. There is an east dipping LVZ revealed by the earthquake signals beneath Taiwan with a velocity of 5.0 km/sec. The shape of the Moho is similar to that in the Southern transect, but the depths are deeper beneath the mountain belts of the Wuyi-Yunkai (~37 km) and Taiwan (~42 km) than in the Southern transect (Figs. 8 and 10).

6. Discussion

In previous studies, the 2D Vp tomography of the T5 transect (Van Avendonk et al., 2014) and 3D Vp tomography (Kuo-Chen et al., 2012a; Cai et al., 2015) only used first arrivals from both active and passive sources for inversion, which have some constraints on reflectors, such as the Moho. In this study, with the benefit of the arrivals of the PmP and PcP phases, we were able to depict the shape of the Moho based on the wide-angle seismic data sets. In general, the velocity distributions from previous studies are consistent with those in this study, and some key crustal features can be summarized as follows: 1) the LVZ extended in the NNE-SSW direction beneath the ZH-DP fault zone of central Fujian (Cai et al., 2015), 2) the HVZ in the lower crust beneath the coastline in southeastern Fujian (Cai et al., 2015), and 3) the LVZ beneath the Central Range in the central Taiwan (Kuo-Chen et al., 2012b; Van Avendonk et al., 2014).

The shape of the Moho has been studied using different geophysical methods, such as gravity modeling (e.g., Hsieh et al., 2010), receiver function (e.g., Ai et al., 2007; Wang, 2010; Tang, 2010; and Li et al., 2013), and seismic travel-time tomography (e.g., Kim et al., 2005; Wu et al., 2007; Kuo-Chen et al., 2012a; Huang et al., 2014; and Cai et al., 2015). Based on the empirical relationship between density and seismic compressional velocity, the results from gravity modeling have shown that the depth of the Moho beneath the coastline of southeastern Fujian is 31-32 km; beneath Penghu Island of the Taiwan Strait, it is ~27 km; and beneath southwestern Taiwan, it is 35 km (Hsieh et al., 2010). Studies from receiver functions have indicated that the depth of the Moho beneath western and central Fujian is 31-32 km (Li et al., 2013); beneath the coastline of Fujian, it is ~30 km (Ai et al., 2007; and Li et al., 2013); beneath Penghu Island, it is 27 km (Tang, 2010); and under the Central Range of Taiwan, it is 44-52 km (Kim et al., 2004). In general, the pattern of the Moho in this study agrees with that from other geophysical studies, which is thicker beneath both the Wuyi-Yunkai and Taiwan orogens than under the Taiwan Strait and the coastline of Fujian, and the thickest crust is under the Taiwan orogen (Fig. 11). Although the styles of convergence cannot be guaranteed based on the incomplete ray coverage, they can be explained based on the differences between the velocity distributions of these 3 transects from the limited datasets. Thus, we assume that they are under different convergence styles because they have different velocity structures. 1) For the Northern transect, the lateral velocity variation in the lower crust from the Taiwan Strait to the island of Taiwan is smoother than the other 2 transects. The low velocity materials in the mid-crust do not enter into the lower crust. No root has been found in the current stage of collision in the Northern transect. 2) For the Middle transect, the low velocity materials extend to a significant depth. A LVZ in the mid-crust beneath the Central Range was resolved. The velocity distribution beneath the island of Taiwan also shows the high-low interbedded layers with an east dipping trend. Ongoing subduction has been found in the Middle transect. 3) For the Southern transect, the lateral velocity change is large in the lower crust. The low velocity materials in the mid-crust extend vertically into the lower crust. Thus, the crust beneath the island of Taiwan is vertically thickened. A root has been found in the current stage of collision. Moreover, from the geological evidence (Ho, 1999), the ages of the crusts in Taiwan increase in age from South to North. Therefore, the evolution of the crustal structures could have occurred by 1) a crustal root was created by collision, 2) the continental crust subducted into the oceanic crust after collision, and 3) the subducted crust was detached from the continental crust. The styles of convergence can be better resolved by integrating with more data covering the east flank of the Moho boundary beneath the island of Taiwan in the future. It is interesting to note that, based on the shape and thickness of the crust beneath two orogens, the thicker and narrower the crustal root, the younger the orogen. For the young Taiwan orogen, due to the strong collision between the Eurasian and Philippine sea plates, the deepest crustal root is not right beneath the highest elevation of the mountain belt but shifts to the west with an asymmetrical bowl pattern (Middle and Southern transects in Fig. 11). In contrast, in the old Wuyi-Yunkai orogen, which is a good comparison with the active Taiwan orogen, the crustal root is not significant in the Middle and Southern transects and does not exist in the Northern transect (Fig. 11).

Southeastern China has been through several stages of tectonic evolution since the Paleozoic era (e.g., Charvet, 2013). The crustal structures obtained in this study not only show the crustal structures revealed by fossil evidence that were created in the Paleozoic and Mesozoic but also verify the current crustal deformation that resulted from the collision between the Eurasian and Philippine sea plates. In the Wuyi-Yunkai mountain belt, the Zhenghe-Dapu (ZH-DP) and the Changle-Zhaoan (CL-ZA) fault zones play important roles in the crustal evolution. The Zhenghe-Dapu suture zone is a deep cutting crustal fault zone, which serves as a boundary from the surface to the lower crust between the Paleozoic and Mesozoic basement (Fig. 11). On the surface, near the ZH-DP fault zone, pelagic sedimentary rocks, basaltic debris, and ophiolite mélange were found in other studies, which suggests that, during the Caledonian orogeny, this region was experiencing extension conditions and developing of an oceanic basin but transitioned into a compression environment during the Indosinian movement (Li, 2013). In the Taiwan mountain belt, the LVZ beneath the Central Range in central Taiwan is a no seismicity area (Kuo-Chen et al., 2012a). Considering the distributed pattern of P wave velocities in this study and the convergence between the Eurasian and Philippines Sea plates in Taiwan, the interpretation from Kuo-Chen et al. (2012b) is preferred: It is hot and dry in the mid-lower crust beneath the Central Range due to the α-β quartz transition instead of a high fluid pressure or partial melting. This conclusion is based on the geophysical evidence of the low Vp/Vs ratio of ~1.55, showing the suitable content of ~22% quartz in the granitic rocks and reasonable geothermal gradient of 30 °C/km above a depth of 24 km, and the high resistivity of ~500 Ohm-m, indicating anhydrous conditions. In contrast, Van Avendonk et al. (2014) suggested that the incoming sediments and upper crust of the Eurasian Plate are buried to mid-crustal depth in the orogen based on the Vp seismic structure. However, if cooler sediments and the upper crust are in the middle crust, it is hard to explain the high-attenuation rocks and lack of seismicity in the mid-crust based on other observations.

As a result, we determined that the crustal structure beneath the ZH-DP fault zone (summary 1) shows a symmetrical step-like structure as a closed oceanic basin structure, and this basin-shape structure is wider towards the north (Fig. 11). Beneath the southern Changle-Zhaoan (CL-ZA) fault zone (summary 2, in the Southern transect), the relatively high-velocity zone up to the upper crust around at a depth of 5 km might correspond to the Neogene tholeiitic basalt only found on the surface (e.g., ChangPu county in Fujian and Kinmen Island), which indicates that, in an extension environment (Li, 2013), this extension force could be related to the South China sea opening (Lu, 2000). In contrast, the crustal structure of the active Taiwan orogen is entire a compare to that of the Wuyi-Yunkai orogen. The LVZ in the mid-crust beneath the Central Range in central Taiwan (summary 3) is dry and hot because

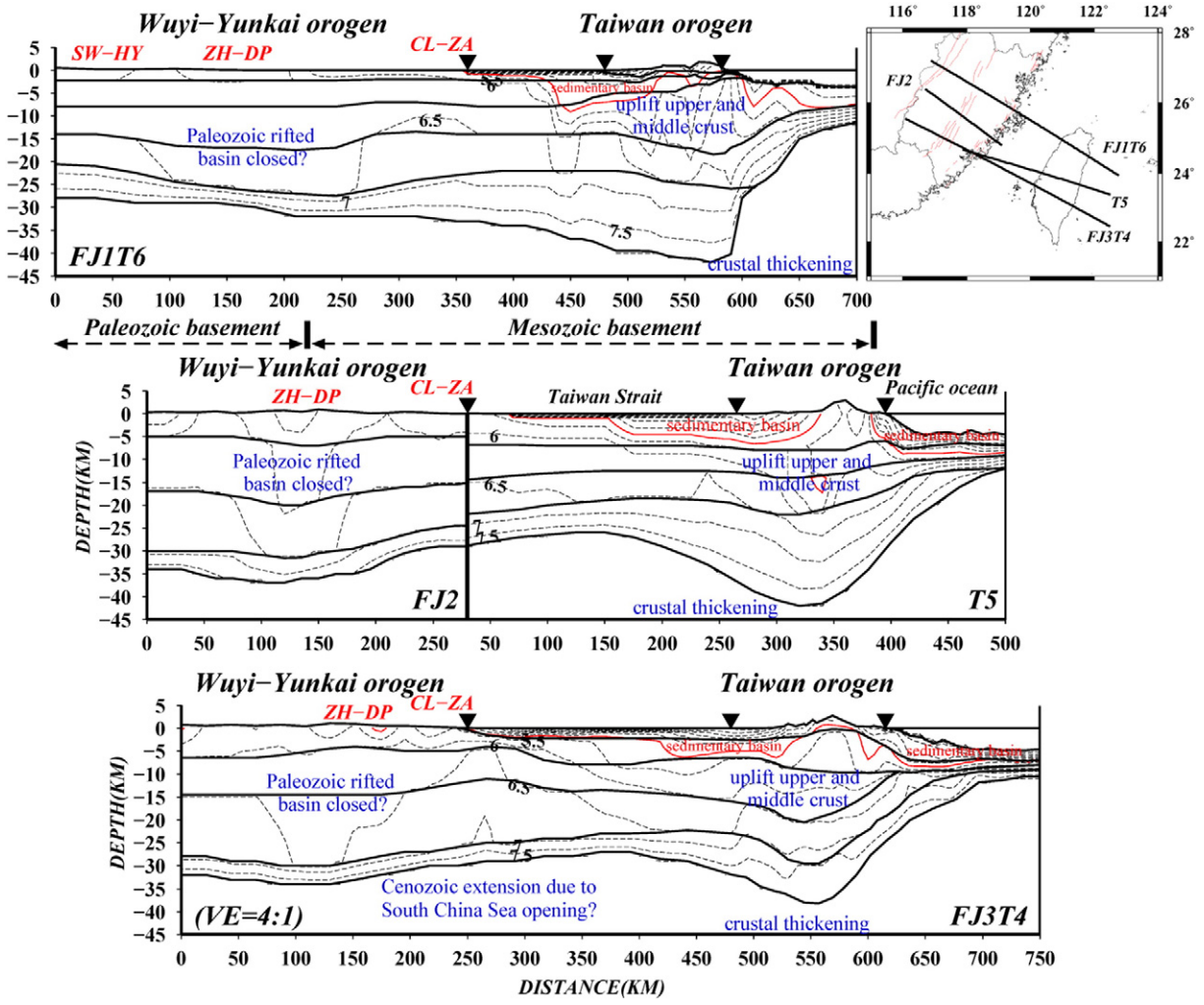

Fig. 11. Three 2D velocity structures across the Taiwan Strait in the North, Middle, and South were generated from this study. The reference point is chosen as the Fujian coastline for understanding as marked by the black solid vertical line in the middle panel. The inversed black triangles mark the locations of the major fault zones in Fujian. The number in the velocity model shows the value of the velocity in the corresponding area. There are 3 features (which are marked by blue characters in the figure) that can be seen in the figure, and the interpretations are as follows: 1) A symmetrical step-like structure as a closed oceanic basin structure showed up beneath the ZH-DP fault zone. 2) An extension force related to the South China Sea opening showed up beneath the southern CL-ZA fault zone. 3) Uplift of the upper and middle crusts on the surface in the mountain belt and significant crustal thickening beneath Taiwan is caused by the fast convergence between EUP and PSP.

of the changes in the compositions of the rocks in the scrapings during subduction under high-graded metamorphism. The fast convergence rate between two plates results in the uplift of the upper and middle crusts on the surface in the mountain belt and significant crustal thickening. In addition, due to the rapid uplift and erosion rates, the sedimentary basins are well developed on both sides of the mountain belt (above the red dashed lines in Fig. 11; the red dashed line shows the 5.0 km/s Vp contour).

7. Conclusions

In this study, we integrated the datasets from the TAIGER and ATSEE projects to resolve onshore-offshore deep crustal seismic profiles from the Paleozoic Wuyi-Yunkai orogen to the Cenozoic Taiwan orogen in southeastern China. In total, three seismic profiles were resolved, and the longest profile is 850 km. Unlike 2D and 3D first arrival traveltime tomography from previous studies, we used both refracted and reflected phases (Pg, Pn, PcP, and PmP) to better model the crustal structures and the crustal reflectors. As a result, the complex crustal evolutions since the Paleozoic era were determined, which involved the Paleozoic rifted basin in Fujian, the Cenozoic extension due to the South China sea opening in the Taiwan Strait, and the on-going collision of the Taiwan orogen.

Acknowledgements

The TAIGER project is a joint USA-Taiwan program in collaboration with Japanese and French scientists. The ATSEE project is a collaboration with scientists in Fujian. This research is supported by the Ministry of Science and Technology in Taiwan and the National Science Foundation in the US. H. K-C was supported by National Science Council (Grant No.: NSC 101-2116-M-008-023-MY3) and Ministry of Science and Technology (Grant No.: MOST 104-2628-M-008-005-MY3). Thanks to PASSCAL for providing seismic instruments and professional technical support. Thanks to the professors and students at NCU, NCCU, NTU, NTOU, and IES in Taiwan and UTIG in the US. Thanks to the researchers that we worked with under the ATSEE project in FJEA in Fujian, China.

References

Ai, Y.S., Chen, Q.F., Zeng, F., Hong, X., Ye, W.Y., 2007. The crust and upper mantle structure beneath southeastern China. Earth Planet. Sci. Lett. 260, 549–563.

Cai, H.T., Kuo-Chen, H., Jin, X., Wang, C.Y., Huang, B.S., Yen, H.Y., 2015. A three dimensional Vp and Vp/Vs crustal structures in Fujian, Southeast China, from active- and passive-sources experiment. J. Asian Earth Sci. http://dx.doi.org/10.1016/j.jseaes.2015.06.014.
Chai, B.H.T., 1972. Structure and tectonic evolution of Taiwan. Am. J. Sci. 272, 389–422. http://dx.doi.org/10.2475/ajs.272.5.389.
Charvet, J., 2013. The Neoproterozoic-early Paleozoic tectonic evolution of the South China block:an overview. J. Asian Earth Sci. 74, 198–209. http://dx.doi.org/10.1016/j.jseaes.2013.02.015.
Chen, W.S., Yang, H.C., Wang, X., Huang, H., 2002. Tectonic setting and exhumation history of the Pingtan-Dongshan Metamorphic Belt along the coastal area, Fujian Province, Southeast China. J. Asian Earth Sci. 20, 829–840.
Eakin, D., McIntosh, K., van Avendonk, H., Lavier, L., Lester, R., Liu, C.-S., Lee, C.-S., 2014. Crustal-scale seismic profiles across the Manila subduction zone: the transition from intra-oceanic subduction to incipient collision. J. Geophys. Res. (Solid Earth) 119, 1–17. http://dx.doi.org/10.1002/2013JB010395.
Grabau, A.W., 1924. Stratigraphy of China, Part 1:Palaeozoic and Older. Geol. Surv. China (528 pp.).
Ho, C.S., 1986. General geological map of Taiwan (Chinese), Cent. Geol. Surv. (164 pp.).
Ho, C.S., 1999. Introduction to the geology of Taiwan (Chinese), Cent. Geol. Surv. (book).
Hole, J.A., 1992. Nonlinear high-resolution three-dimensional seismic travel time tomography. J. Geophys. Res. 97, 6553–6562.
Hsieh, H.H., Yen, H.Y., Shih, M.H., 2010. Moho depth derived from gravity data in the Taiwan Strait area. Terr. Atmos. Ocean. Sci. 21, 235–241.
Huang, H.H., Wu, Y.M., Song, X.D., Chang, C.H., Lee, S.J., Chang, T.M., Hsieh, H.H., 2014. Joint Vp and Vs tomography of Taiwan: Implications for subduction-collision orogeny. Earth Planet. Sci. Lett. 392, 177–191. http://dx.doi.org/10.1016/j.epsl.2014.02.026.
Jahn, B.M., Chen, P.Y., Yen, T.P., 1976. Rb-Sr ages of granitic rocks in southeastern China and their tectonic significance. Geol. Soc. Am. Bull. 86, 763–776.
Kim, K.H., Chiu, J.M., Pujol, J., Chen, K.C., Huang, B.S., Yeh, Y.H., Shen, P., 2005. Three-dimensional Vp and Vs structural model associated with the active subduction and collision tectonics in the Taiwan region. Geophys. J. Int. 162, 204–220.
Kuo-Chen, H., Wu, F.T., Okaya, D., Huang, B.-S., Liang, W.-T., 2009. SKS/SKKS Splitting and Taiwan Orogeny. Geophys. Res. Lett. 36 (12), 5, L12303. http://dx.doi.org/10.1029/2009GL038148.
Kuo-Chen, H., Wu, F.T., Roecker, S.W., 2012a. Three-dimensional P velocity structures of the lithosphere beneath Taiwan from the analysis of TAIGER and related seismic datasets. J. Geophys. Res. 117 (B06306) (19 pp.).
Kuo-Chen, H., Wu, F.T., Jenkins, D.M., Mechie, J., Roecker, S., Wang, C.-Y., Huang, B.-S., 2012b. The seismic signature of the a-b quartz transition beneath the mountain belts of Taiwan: observed from dense seismic arrays and three-dimensional Vp/Vs tomography. Geophys. Res. Lett. 39 (22), 6, L22302. http://dx.doi.org/10.1029/2012GL053649.
Kuo-Chen, H., Sroda, P., Wu, F.T., Wang, C.-Y., Kuo, Y.W., 2013. Seismic anisotropy of the upper crust in the mountain ranges of Taiwan from the TAIGER explosion experiment. Terr. Atmos. Ocean. Sci. 24, 963–970. http://dx.doi.org/10.3319/TAO.2013.07.30.01(T).
Lester, R., McIntosh, K., 2012b. Multiple attenuation in crustal-scale imaging: examples from the TAIGER marine reflection data set. Mar. Geophys. Res. 33, 289–305. http://dx.doi.org/10.1007/s11001-012-9149-1.
Lester, R., Lavier, L., McIntosh, K., van Avendonk, H., Wu, F., 2012a. Active extension in Taiwan's precollision zone: A new model of plate bending in continental crust. Geology 40, 831–834. http://dx.doi.org/10.1130/G33142.1.
Lester, R., McIntosh, K., van Avendonk, H., Lavier, L., Liu, C.-S., Wang, T.-K., 2013. Crustal accretion in the Manila trench accretionary wedge at the transition from subduction to mountain-building in Taiwan. Earth Planet. Sci. Lett. 375, 430–440. http://dx.doi.org/10.1016/j.epsl.2013.06.007.
Li, X., 2013. Subdivision and characteristic of tectonic units in Fujian Province. Glob. Geol. 32 (3), 549–557.
Li, Q.S., Gao, R., Wu, F.T., Guan, Y., Ye, Z., Liu, Q.M., Kuo-Chen, H., He, R.Z., Li, W.H., Shen, X.Z., 2013. Seismic structure in the southeastern China using teleseismic receiver functions. Tectonophysics 606, 24–35.
Lu, H.J., 2000. Background of seismotectonics of major earthquakes in the sea area southeast of Jinmen (Chinese). Seismol. Geol. 22, 104–110.
Ma, K.F., Wang, J.H., Zhao, D., 1996. Three dimensional seismic velocity structure of the crust and uppermost mantle beneath Taiwan. J. Phys. Earth 44, 85–105.
Mao, J.R., Li, Z.L., Ye, H.M., 2014. Mesozoic tectono-magmatic activities in South China: Retrospect and prospect. (Chinese). Sci. China Earth Sci. 57, 2853–2877. http://dx.doi.org/10.1007/s11430-014-5006-1.
McIntosh, K., Nakamura, Y., Wang, T.K., Shih, R.C., Chen, A., Liu, C.S., 2005. Crustal-scale seismic profiles across Taiwan and the western Philippine Sea. Tectonophysics 401, 23–54.
McIntosh, K., Liu, C.-S., Lee, C.-S., 2012. Introduction to the TAIGER special issue of Marine Geophysical Research. Mar. Geophys. Res. 33, 285–287.
McIntosh, K., Van Avendonk, H., Lavier, L., Lester, R., Eakin, D., Wu, F., Liu, C.-S., Lee, C.-S., 2013. Inversion of a hyper-extended rifted margin in the southern Central Range of Taiwan. Geology 41, 871–874. http://dx.doi.org/10.1130/G34402.1.
McIntosh, K., Lavier, L., Van Avendonk, H., Lester, R., Eakin, D., Liu, C.-S., 2014. Crustal structure and inferred rifting processes in the northeast South China Sea. Mar. Pet. Geol. 58, 612–626. http://dx.doi.org/10.1016/j.marpetgeo.2014.03.012.
Okaya, D., Wu, F., Wang, C.Y., Yen, H.Y., Huang, B.S., Brown, L., Liang, W.T., 2009. Joint Passive/Controlled Source Seismic Experiment across Taiwan. Eos. Trans. 90 (34), 289.
Rau, R.J., Wu, F.T., 1995. Tomographic imaging of lithospheric structures under Taiwan. Earth Planet. Sci. Lett. 135, 517–532.
Roecker, S.W., Yeh, Y.H., Tsai, Y.B., 1987. Three-dimensional P and S wave velocity structures beneath Taiwan:Deep structure beneath an arc-continent collision. J. Geophys. Res. 92, 10547–10570.
Shih, R.C., Lin, C.H., Lai, H.L., Yeh, Y.J., Huang, B.S., Yen, H.Y., 1998. Preliminary crustal structures across central Taiwan from modeling of the onshore-offshore wide-angle seismic data. Terr. Atmos. Ocean. Sci. 9 (3), 317–328.
Shu, L.S., 2012. An analysis of principal features of tectonic evolution in South China Block. (Chinese). Geol. Bull. China 31 (7), 1035–1053.
Shu, L.S., Faure, M., Yu, J.H., Jahn, B.M., 2011. Geochronological and geo-chemical features of the Cathaysia block (South China): new evidence for the Neopro-terozoic breakup of Rodinia. Precambrian Res. 187 (3-4), 263–276. http://dx.doi.org/10.1016/j.precamres.2011.03.003 (<insu-00576470>).
Suppe, J., 1984. Kinematics of Arc-continent Collision, Flipping of Subduction, and Back-arc Spreading Near Taiwan. Mem. Geol. Soc. China 6, 21–33.
Tang, C.C., 2010. The crustal structure of Taiwan from Radial Receiver Function and Triggered Tremor Ph.D. thesis, National Chung Cheng Univ. of R.O.C (133 pp.).
Tapponnier, P., Molnar, P., 1977. Active Faulting and Tectonics in China. J. Geophys. Res. 82 (20), 2905–2930.
Van Avendonk, H., Kuo-Chen, H., McIntosh, K., Lavier, L., Okaya, D., Wu, F., Wang, C.-Y., Lee, C.S., Liu, C.S., 2014. Deep crustal structure of an arc-continent collision: Constraints from seismic travel times in central Taiwan and the Philippine Sea. J. Geophys. Res. 119 (11), 8397–8416. http://dx.doi.org/10.1002/2014JB011327.
Wang, H.L., 2010. A Study on Crust and Uppermost Mantle Structures from Receiver Functions in Taiwan Ph.D. thesis, National Chung Cheng Univ. of R.O.C (118 pp.).
Wu, Y.M., Chang, C.H., Zhao, L., Shyu, J.B.H., Chen, Y.G., Sieh, K., Avouac, J.P., 2007. Seismic tomography of Taiwan: Improved constraints from a dense network of strong motion stations. J. Geophys. Res. 112 (B08312). http://dx.doi.org/10.1029/2007JB004983 (14 pp.).
Wu, F.T., Kuo-Chen, H., McIntosh, K.D., 2014. Subsurface imaging, TAIGER experiments and tectonic models of Taiwan. J. Asian Earth Sci. 90, 173–208. http://dx.doi.org/10.1016/j.jseaes.2014.03.024.
Xu, X.S., O'Reilly, S.Y., Griffin, W.L., Wang, X.L., Pearson, N.J., He, Z.Y., 2007. The crust of Cathaysia: Age, assembly and reworking of two terranes. Precambrian Res. 158, 51–78.
Yeh, Y.H., Shih, R.C., Liu, C.H., Yen, H.Y., Huang, B.S., Liu, C.S., Chen, P.Z., Huang, C.S., Wu, C.J., Wu, F.T., 1998. Onshore/offshore wide-angle deep seismic profiling in Taiwan. Terr. Atmos. Ocean. Sci. 9, 301–316.
Yu, S.B., Chen, H.Y., Kuo, L.C., Lallemand, S.E., Tsien, H.H., 1997. Velocity field of GPS stations in the Taiwan area. Tectonophysics 274 (1–3), 41–59.
Zelt, C.A., Forsyth, D.A., 1994. Modeling wide-angle seismic data for crustal structure: Southeastern Grenville province. J. Geophys. Res. 89, 11687–11704.
Zelt, C.A., Smith, R.B., 1992. Seismic traveltime inversion for a 2D crustal velocity structure. Geophys. J. Int. 108, 16–34.
Zheng, H.W., Gao, R., Li, T.D., Li, Q.S., He, R.Z., 2013. Collisional tectonics between the Eurasian and Philippine Sea plates from tomography evidences in Southeast China. Tectonophysics 606, 14–23.
Zhou, S.Y., Wu, Y., Shi, S.Y., Yang, F.P., 2001. Integrated research on current crustal movement and earthquake dynamics in marginal sea, Southeast of China continent (Chinese) Crustal Deform. Earthq. Vol. 21.